Microstructure and mechanical properties of $(Cr_xTi_{1-x})_2AlC$ 211 MAX phases as composites through spark plasma sintering

Leila Hemati [a], Mohammad Farvizi [a, *], Sayed Alireza Ataie [b, *], Leila Nikzad [a], Ehsan Ghasali [c, d], Arash Faraji [a], Tomasz Liskiewicz [e]

[a] Department of Ceramic, Materials and Energy Research Center, Karaj 31787-316, Iran

[b] Iran University of Science and Technology, School of Metallurgy and Materials Engineering, Narmak, Tehran 16846–13114, Iran

[c] College of Geography and Environmental Sciences, Zhejiang Normal University, Jinhua, 321004, China

[d] College of Chemistry and Material Sciences, Zhejiang Normal University, Jinhua, 321004, Zhejiang, China

[e] Department of Engineering, Faculty of Science and Engineering, Manchester Metropolitan University, Manchester M1 5GD, UK

[*]Corresponding Author: M. Farvizi

Email: mmfarvizi@yahoo.com, mmfarvizi@merc.ac.ir

Fax: +98-21-88773352; Tel: +98-935 848 5439

ORCID ID: https://orcid.org/0000-0003-3225-4788

Abstract

MAX phases are intriguing materials due to their unique properties. However, each of these materials possesses its own weaknesses when subjected to service conditions. For example, while one MAX phase exhibits self-lubricating feature, it may not perform well under high load conditions. This study investigates the impact of adding chromium to Ti_2AlC on microstructure and mechanical properties. Samples are prepared through ball-milling and spark plasma sintering (SPS), then analyzed using various techniques. The presence of different phases, including MAX phases (Ti_2AlC and Cr_2AlC), carbides (TiC and Cr_7C_3), and low amounts of oxides, is identified. Hardness, fractography, and wear characteristics are assessed through indentation and sliding tests. The study correlates the wear rate of each sample with experimental (H/E) and theoretical indicators (B/G), showing the production of composites with improved properties suitable for diverse applications.

Keywords: Spark Plasma Sintering (SPS); MAX phase; Composite; Hardness; Wear.

1. Introduction

MAX phases are a family of ternary nitrides and carbides which generally crystallize with hexagonal P63/mmc structure in the general formula of $M_{n+1}AX_n$ (n = 1, 2, or 3), where “M” is a transition metal, “A” is an A-group element, and “X” is either C or N [1,2]. These materials find applications in various industries, including oxidation resistance [3,4], magnetization [5], thermal-shock or high-temperature resistance [6,7], optics [8], nuclear [9], anti-corrosive [10], anti-wear and self-lubricating materials [11,12]. The diverse applications of MAX phases are attributed to their various intrinsic properties. The well-known strength and mechanical properties of these phases are particularly intriguing, as they usually possess self-healing capabilities [13,14] and better damage tolerance compared to other ceramics (these materials do not exhibit high hardness/Young's modulus, therefore they are less brittle compared to other ceramics) [15,16]. Also, MAX phases show outstanding properties such as low thermal expansion coefficient, low density, great resistance to thermal variations similar to ceramics, good electrical and thermal conductivity and proper machinability like the metals [17-20]. Introducing MAX phases for the first time in 1960s by Nowotny et al. [21,22] with the name of "H-phase materials" and developing them at the beginning of 1990s, by Barsoum et al. [23] leads to pay more attention on this new group of materials which combines some features of metals and ceramics simultaneously. However, the unique properties of these materials have likely contributed to increased research interest in these phases since the year 2000. Fig. 1 depicts the statistical analysis of scientific papers published between 1990 and 2023, obtained using titles or topics containing the keywords "MAX phase" and "mechanical properties". The data (particularly the trend in citations) indicates an acceleration in the study of the mechanical properties of these materials since 2015.

Different type of products (powders, bulk materials and coatings) as well as synthesis methods have been introduced relating to the MAX phases [24-27]. One of the most important parameters in the production of MAX phases is the heating method or in other words sintering

process [28,29]. It has been approved that normally, a pressure assisted sintering method such as hot pressing and SPS can led to the preparation of relatively high purity products than other sintering methods. This can be justified as a simple reality that MAX phases formation needs high diffusion rate of reactants [30-32]. Therefore, a mass transportation of components of MAX phases as a result of applied pressure and elevated temperature can guarantee a higher possibility for the presence of desired composition [33,34]. In the other word, the binary contact of components leads to the formation of intermetallics or carbides regions which can be transformed to MAX phase at the final stage of the sintering process [35,36]. Consequently, it can be recognized from the literature review that spark plasma sintering with unique advantages such as vacuum condition, sparks between particles, high heating rate, and applied pressure is considered promising method for the production of MAX phases [37,38].

MAX phases have various types, such as 413 (M_4AX_3), 312 (M_3AX_2) and 211 (M_2AX) but the 211 type (where M represents Nb, Mn, Sc, V, Ti, and Cr) are more commonly investigated [39,40]. Among 211 MAX phases, Ti_2AlC and Cr_2AlC are more extensively studied for protective applications probably due to the low density (conversely the density of Nb_2AlC was reported 6.37 $g.cm^{-3}$ [40]), facile synthesis method, multi-functionality and inexpensive raw materials [41-44]. Ti_2AlC exhibits a notable healing effect due to the formation of Al_2O_3 [14], but it demonstrates relatively low strength attributed to its inferior elastic constants [45] and the presence of crack gaps that can facilitate failure [14]. Also, Ti_2AlC is considered as the lightest Ti-based MAX phase in the 211 ordering with a density of 4.11 g/cm^3 [46]. Zhou et al. [47] prepared high-purity Ti_2AlC MAX phase through spark plasma sintering of Ti-Al-C powder mixture at 1100˚C with Vickers hardness of 4 GPa. Ping et al. [48] reported mechanical properties of Ti_2AlC MAX phases, prepared through hot pressing of TiC, Al, Ti, and carbon active powders at 1400˚C, including bending strength, compressive strength, fracture toughness, and hardness at room temperature as 384 MPa, 670 MPa, 7 $MPa.m^{0.5}$, and 4.2~5.7 GPa, respectively. Cai et al. [49] produced Ti_2AlC via hot pressing at 1450˚C for 30 min at applied pressure of 28 MPa. The tribological behavior of this compound against low carbon

steel pins under normal load of 20–80 N showed a friction coefficient of 0.3–0.45 and a wear rate of (1.64–2.97) $\times 10^{-6}$ mm^3/N.m. Cr_2AlC displays high corrosion resistance at elevated temperatures [50]. Tian et al. [51,52], Ying et al. [53], and Li et al. [54] synthesized Cr_2AlC ceramics with nearly high hardness (more than 6 GPa), considerable flexural (more than 480 MPa) and superior compressive strength (more than 949 MPa), using ball milling and hot-press techniques. Several studies [55-60] have investigated the dry sliding behavior of MAX phases, particularly in Cr/Ti-Al-C systems, to determine the presence of self-lubricating and self-healing properties. However, it is significant to mention that these studies have primarily focused on the sliding characteristics of MAX phases under low loads, typically below 20 N. In addition, in the case of composite materials, it is important to note that the density and the nature of phases in multi-component systems can influence hardness measurements and behavior. For instance, increased densities may result in greater hardness [61]. In cases where metallic phases coexist with ceramic phases, it is advisable to provide mechanical maps to account for potential plasticity or interface effects that may impact the hardness and Young's modulus data [62,63].

As well as ternary MAX Phases, quaternary MAX phases or solid solution of them, denoted as $(M_{1-x}M'_x)_{n+1}AX_n$ (x=0-1), have also been synthesized for tailoring of new compounds with improved physical and mechanical properties such as considerable fracture toughness, strength, hardness and oxidation resistance [64-67]. For example, Tunca et al. [64] synthesized $(Zr_{1-x}Ti_x)_2(Al_{0.5}Sn_{0.5})C$ MAX phase by reactive hot pressing and showed that the partial replacement of Al by Sn at A site can facilitate the formation of high-purity products. Also, in other study [65], the solid solution $(Zr_{1-x}Nb_x)_2AlC$ MAX phase exhibited higher bond strength, hardness, and greater shear deformation resistance than Zr_2AlC. Liu et al. [66] synthesized successfully two new MAX compounds: $(Cr_{2/3}Ti_{1/3})_3AlC_2$ and $(Cr_{5/8}Ti_{3/8})_4AlC_3$ by hot pressing in Ti-Cr-Al-C system. Also, they synthesized [67] quaternary MAX phase: $(Cr_{2/3}Ti_{1/3})_3AlC_2$ via reaction between Cr_2AlC and TiC and investigated the crystal structure and formation mechanism of it. Also, this system could significantly enhance the inherent safety factor of

nuclear reactors during operation [68]. Further, several studies have examined the theoretical and experimental formation of phases in the Cr-Ti-Al-C system [69-75]. All things considered, the $(CrxTi1\text{-}x)_2AlC$ system may present an advantageous option for a material with high self-healing, self-lubrication, toughness and strength.

To the best of the authors' knowledge, there are no research studies related to the preparation of MAX phases in the Cr-Ti-Al-C composite system via spark plasma sintering, as well as a detailed investigation of their mechanical (e.g., fractography) and wear properties. Therefore, the present study initially explores the impact of Cr addition on the microstructure and phase formation of Ti_2AlC MAX phases by various characterization methods. Subsequently, the mechanical and wear properties of $(Cr_xTi_{1-x})_2AlC$ systems are examined. Finally, the wear characteristics of each sample are correlated with the microstructure and mechanical parameters.

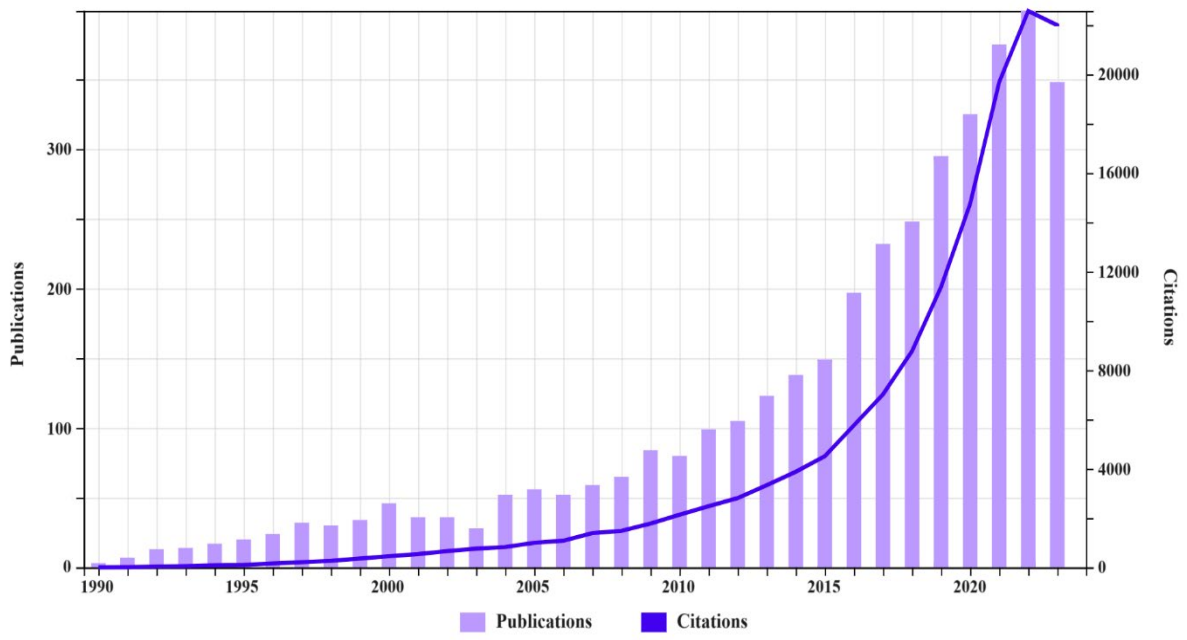

Fig. 1: Statistical data of research publications from 1990 to 2023 was compiled from the Web of Science using the keywords "MAX phase" and "mechanical properties".

2. Experimental procedure

2.1. Materials and samples

Ti (Alfa Aesar, Germany, 99.6%), Cr ((Merck, 99.9%), Al (Merck, 99.9%), and carbon black powders were used as starting materials. The morphology of used raw materials is illustrated in Fig. 2a. Further, for a more comprehensive view, the phase diagram and crystal structure of possible intermetallic, carbide and MAX phases are depicted in Fig. 2b. Five different batches of powders mixture including $(Cr_xTi_{1-x})_2AlC$, where x is 1, 0.75, 0.5, 0.25 and 0 have been selected. Therefore, five samples with the final composition of Ti_2AlC, $(Cr_{0.25}Ti_{0.75})_2AlC$, $(Cr_{0.5}Ti_{0.5})_2AlC$, $(Cr_{0.75}Ti_{0.25})_2AlC$ and Cr_2AlC were mixed by a high energy ball mill in stainless steel cup at argon atmosphere for 8 h. It is important to note that in order to achieve the 211 (M+M')AX phase system, the ratio was set to be 2:1.05:0.95 (like Ref. [72]). This adjustment was necessary to remunerate for the Al sublimation that occurs between its melting and reaction with graphite. The selection of processing parameters such as milling conditions and sintering temperature was done according to Ref. [37]. After the milling process, the mixtures were inserted directly into graphite mold and the SPS process was performed with initial and final pressures of 10 and 30 MPa, respectively with proper vacuum condition of 10 Pa. The SPS process was conducted at maximum sintering temperature of 1100 °C with an average heating rate of 78 °C/min and for 30 min as soaking time at maximum temperature. During this process, the stable phases may include Ti_2AlC (crystal lattice is hexagonal and space group is $P6_3/mmc$), TiC (cubic, Fm-3m), Cr_2AlC (hexagonal, $P6_3/mmc$), and Cr_7C_3 (orthorhombic, Pmcn:bca), as illustrated in Fig. 2c. Fig. 3 depicts the variation of punch displacement and temperature during the SPS procedure. After the sintering process, the samples were grounded carefully to remove graphite foils. Further, to omit/disperse excess carbon and the undesired phase ($Cr_{23}C_7$) in the SPS process, it is recommended to subject the samples to annealing at temperatures above 1000°C [76,77].

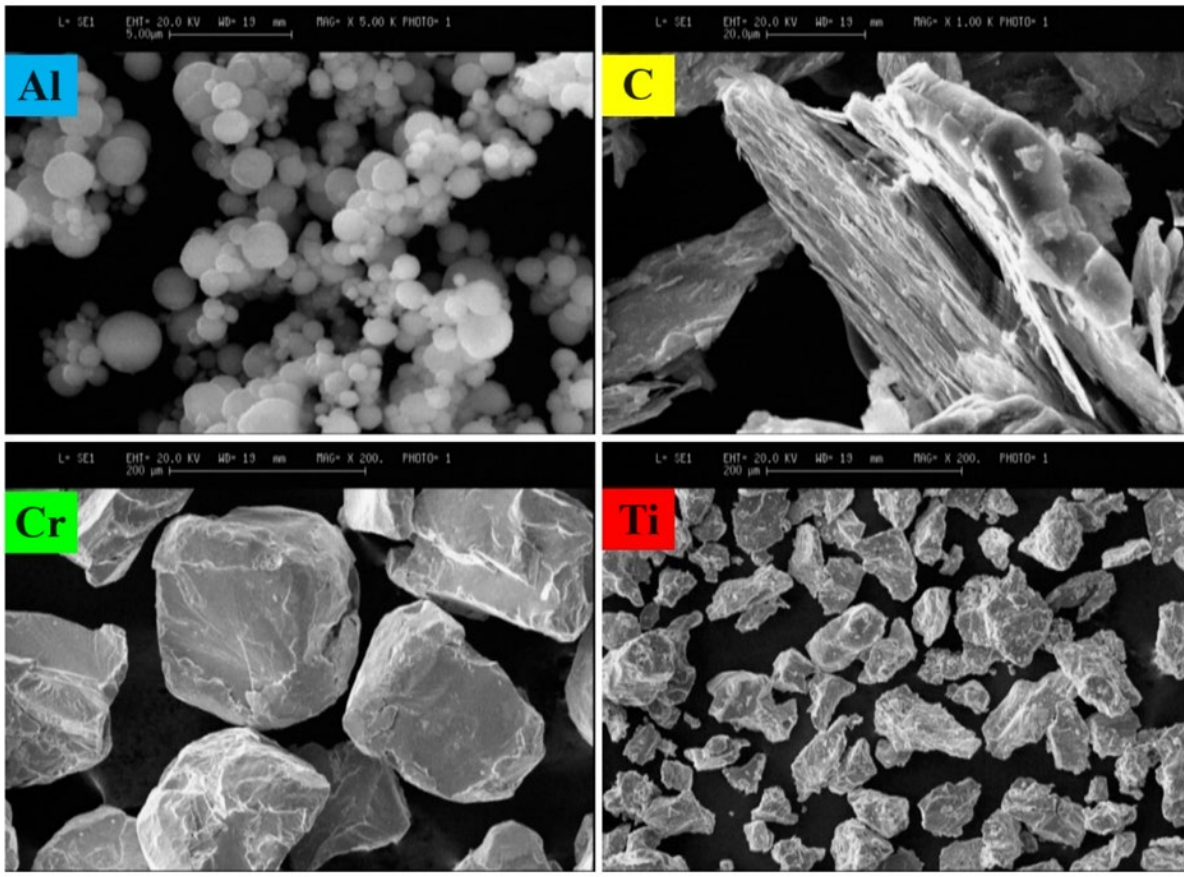

(a)

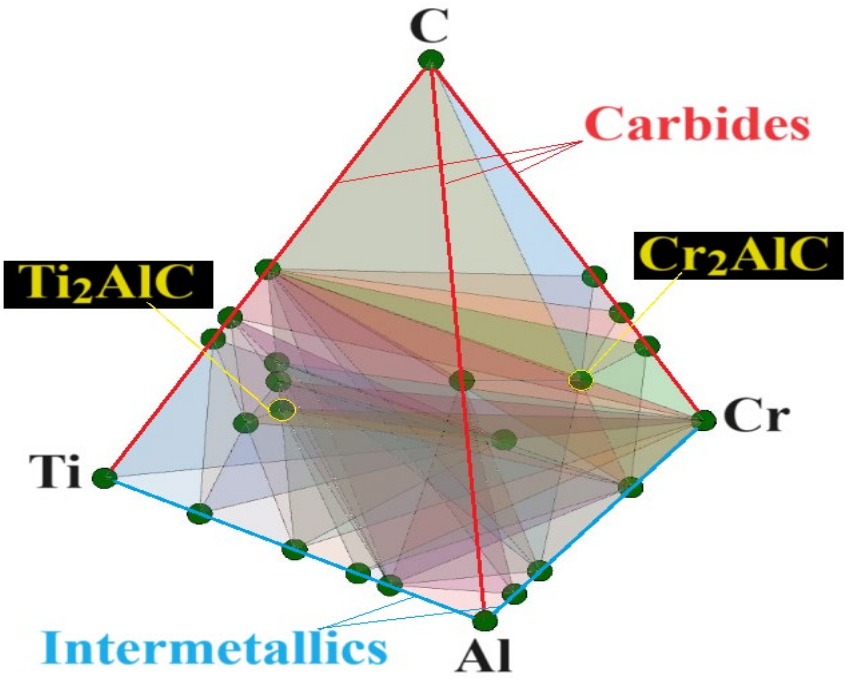

(b)

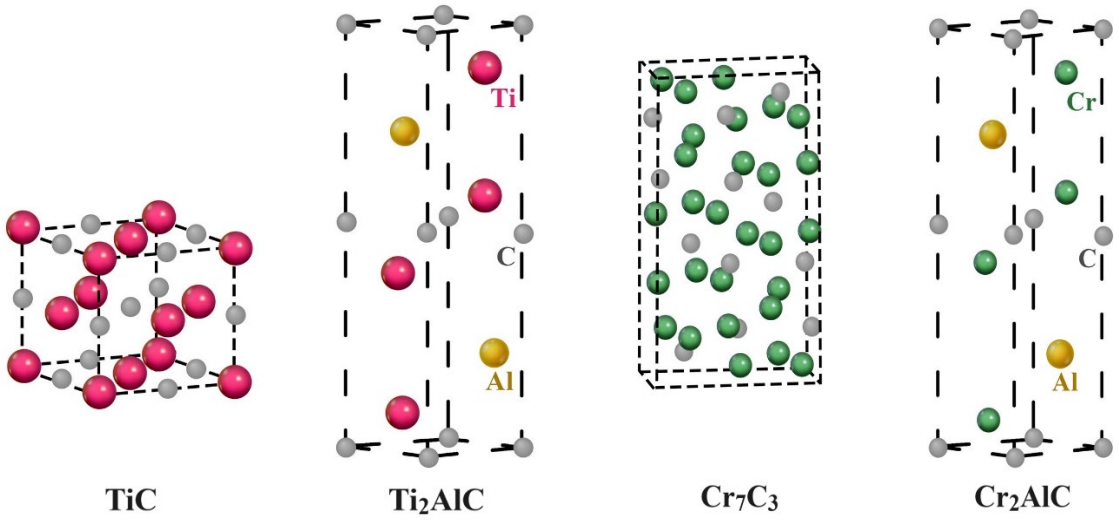

(c)

Fig. 2: (a) SEM micrographs of raw materials; (b) Phase diagram of Ti-Cr-Al-C system (c) Atomic crystal structure of Ti_2AlC, Cr_2AlC, TiC and Cr_7C_3 phases

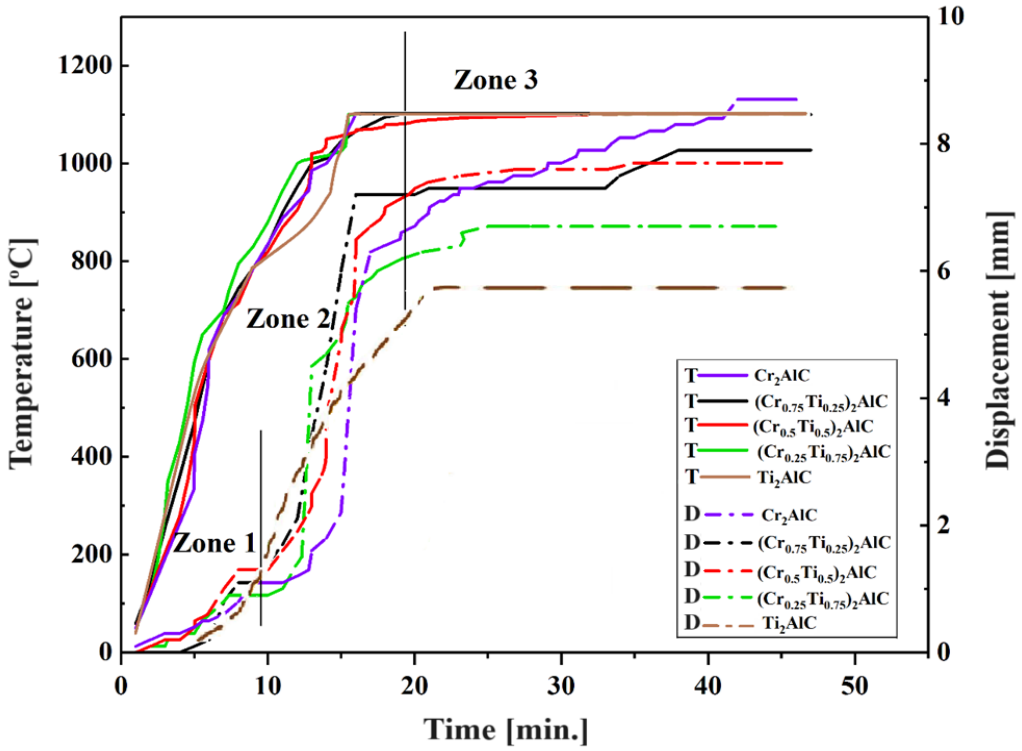

Fig. 3: Temperature and punch displacement variation as a function of sintering time for each sample

2.2.Characterization techniques

Scanning electron microscope equipped with EDS (MIRA 3 TESCAN, Czech Republic, Stereoscan 360, Leica Cambridge) was used to observe the chemistry and morphology of the synthesized samples. The phase analysis of the samples was performed by X-ray diffraction (Philips-PW3710) in the 2θ range of 20–80° with Cu K_α radiation (λ = 1.54 A°) at 40 kV. Based on the XRD patterns, the crystallographic and quantitative analysis of samples were performed using Rietveld refinement method by Materials Analysis Using Diffraction (MAUD) software. Additionally, to examine the phase structure of samples, Raman spectroscopy (Uni-DRON, South Korea) was used. Laser wavelength was 532 nm and resolution was 1 cm^{-1}. To improve the signal-to-noise ratio, the acquisition time was set at 5 minutes, and spectra were calibrated employing a silicon plate. For each sample, the density/porosity level was taken based on the ASTM B962-23 [78]. The nanoindentation test was carried out via Nano Indenter Specification TB26375 with a maximum load of 10 mN and a holding time of 5 s. The Hardness and Young's modulus were calculated using Oliver-Pharr equations [79]. At least ten indentations from different locations were made for each sample to enhance accuracy and reliability. A homemade three-point bending test was conducted at a cross-head speed of 0.2 mm/min using specimens with dimensions of 25 x 2 x 2 mm in order to examine the fracture surface. In order to investigate the wear properties of the samples, a pin-on-disk method was used at room temperature according to the ASTM G99-05 standard. The humidity level was 30%, and no lubrication was applied. A tungsten carbide pin with a diameter of 10.3 mm was used as the counter friction pair. The applied normal load during wear was 30 N, with a sliding distance of 100 m (3287 rounds). The friction coefficient was determined by the sensors in the abrasion device. After completing the test, in order to review and analyze the results, the worn surface was examined by field emission scanning electron microscope (FESEM). Then wear rate was determined via this formula: Wear rate = V / (N.S), Where "V" is the volume loss of the specimen (mm^3), "N" is the normal load (N), and "S" is the sliding distance (m). The Volume

loss was calculated via (V) = (πRd^3) / 6r, where "R" is the wear track radius (mm), "d" denotes the wear track width (mm), and "r" represents the pin radius (mm) after wear tests [80,81].

3. Results and discussions

3.1. Microstructure

The XRD patterns in Fig. 4 illustrate the phases present in the prepared samples. In Fig. 4a, the primary crystalline phase corresponds to the Ti_2AlC MAX phase, with additional minor peaks corresponding to the TiC by-product. The substitution of Ti with Cr results in the formation of peaks related to Cr_2AlC, as well as carbide compounds such as TiC and Cr_7C_3. This phase structure is in good agreement with the other Ref. [74]. However, in contrast to the XRD findings reported in references [72,73], XRD patterns of our samples did not exhibit the presence of intermetallic and 312 MAX phases. To gain a comprehensive understanding of the impact of Cr addition on the phase structure in the Ti-Al-C system and to confirm the peak positions, Rietveld refinement analysis was conducted on the samples. The results of this analysis are depicted in Figs. 5 and 6 (for detailed analysis Table 1 is presented). The investigation of the Ti_2AlC sample reveals the presence of 95.4 wt.% MAX phase and 4.6 wt.% TiC. Upon the addition of 0.25 mol.% of Cr to the Ti-Al-C system, the corresponding XRD pattern shows the presence of Ti_2AlC (53.9 wt.%), TiC (14.6 wt.%), and Cr_2AlC (31.3 wt.%). Interestingly, in the $(Cr_{0.5}Ti_{0.5})_2AlC$ and $(Cr_{0.75}Ti_{0.25})_2AlC$ samples, the absence of Ti_2AlC peaks is observed, with these samples mainly consisting of Cr_2AlC and TiC phases. The content of Cr_2AlC increases with higher Cr content. As expected, the last sample exclusively contains Cr_2AlC (97.2 wt.%) and Cr_7C_3 phases (2.7 wt.%). Further, it is evident that the addition of chromium to Ti_2AlC leads to a higher percentage of the TiC phase.

A closer examination of the peak positions of MAX phases indicates a slight shift towards higher diffraction angles with the addition of 25 mol.% Cr, which can be attributed to the smaller atomic radius of Cr compared to Ti, leading to a reduction in lattice parameters in the

Ti_2AlC structure. This issue is also evident in Table 1. The appearance of Cr_2AlC peaks alongside Ti_2AlC peaks suggests that the formation of a complete solid solution did not occur in the $(Cr_{0.25}Ti_{0.75})_2AlC$, $(Cr_{0.5}Ti_{0.5})_2AlC$, and $(Cr_{0.75}Ti_{0.25})_2AlC$ samples due to the amount of soluble atoms (either Cr or Ti in the M-Al-C system) exceeding the saturation limit (less than 20 at. % [4,75]). Additionally, as the chromium content in the samples increases, Cr_2AlC peaks exhibit a slight shift towards lower angles in the corresponding XRD patterns, which can be explained by the atomic radius difference between titanium and chromium components.

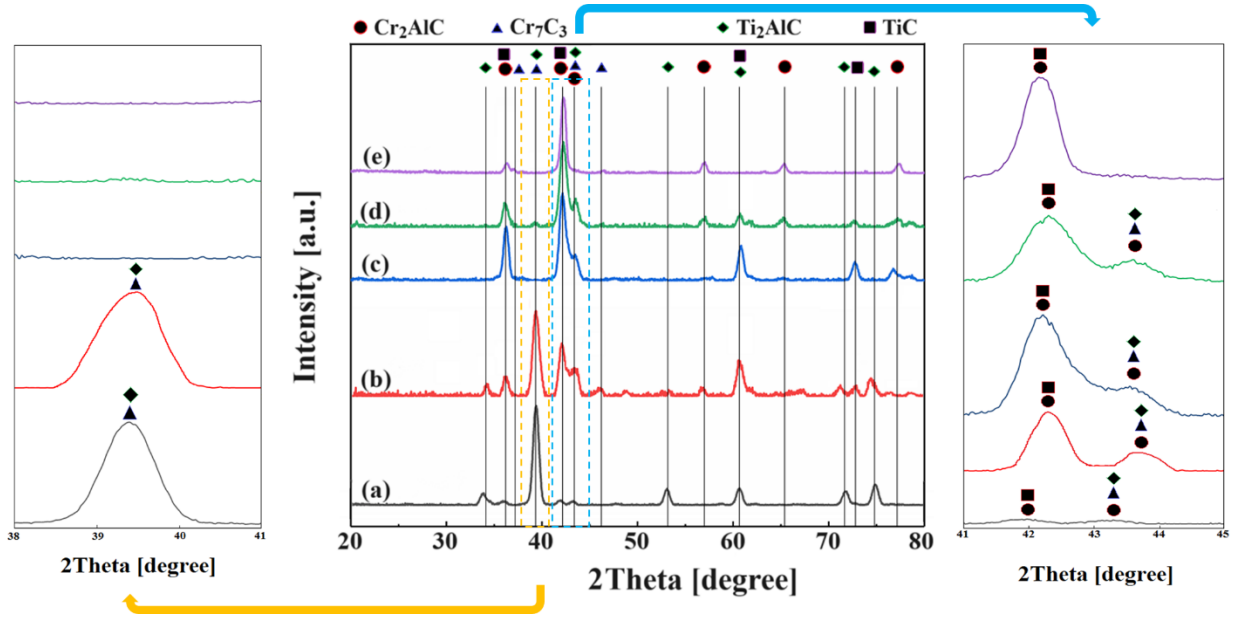

Fig. 4: XRD patterns of Ti_2AlC MAX phase with different amounts of Cr addition of (a) Ti_2AlC, (b) $(Cr_{0.25}Ti_{0.75})_2AlC$, (c) $(Cr_{0.5}Ti_{0.5})_2AlC$, (d) $(Cr_{0.75}Ti_{0.25})_2AlC$ and (e) Cr_2AlC. PDF cards: Ti_2AlC (29-0095), Cr_2AlC (29-0017), TiC (32-1383), and Cr_7C_3 (00-036-1482)

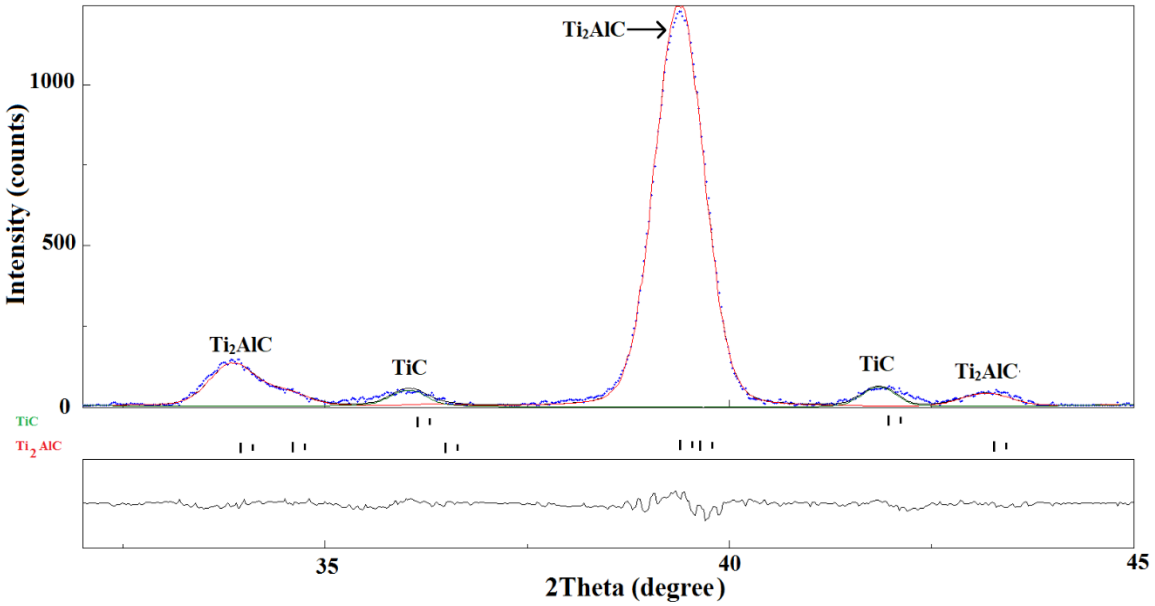
Ti2AlC
1000
500
0
Intensity (counts)
Ti2AlC
TiC
TiC
Ti2AlC
TiC
Ti2AlC
35
40
45
2Theta (degree)

(a)

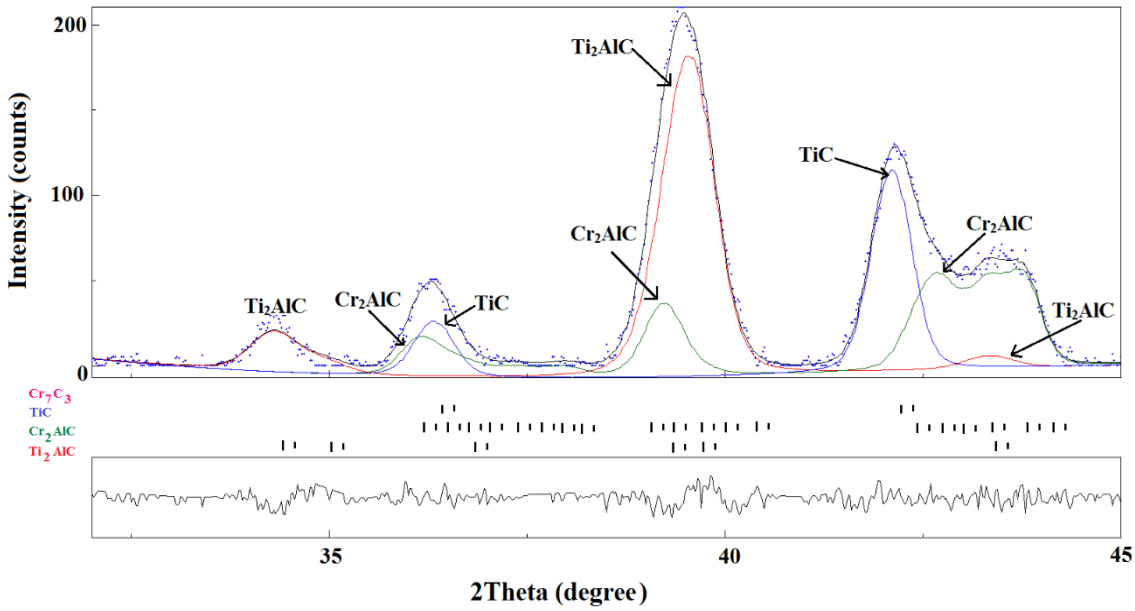
200
100
0
Intensity (counts)
Ti2AlC
Cr2AlC
TiC
Ti2AlC
Cr2AlC
TiC
Cr2AlC
Ti2AlC
Cr7C3
TiC
Cr2AlC
Ti2AlC
35
40
45
2Theta (degree)

(b)

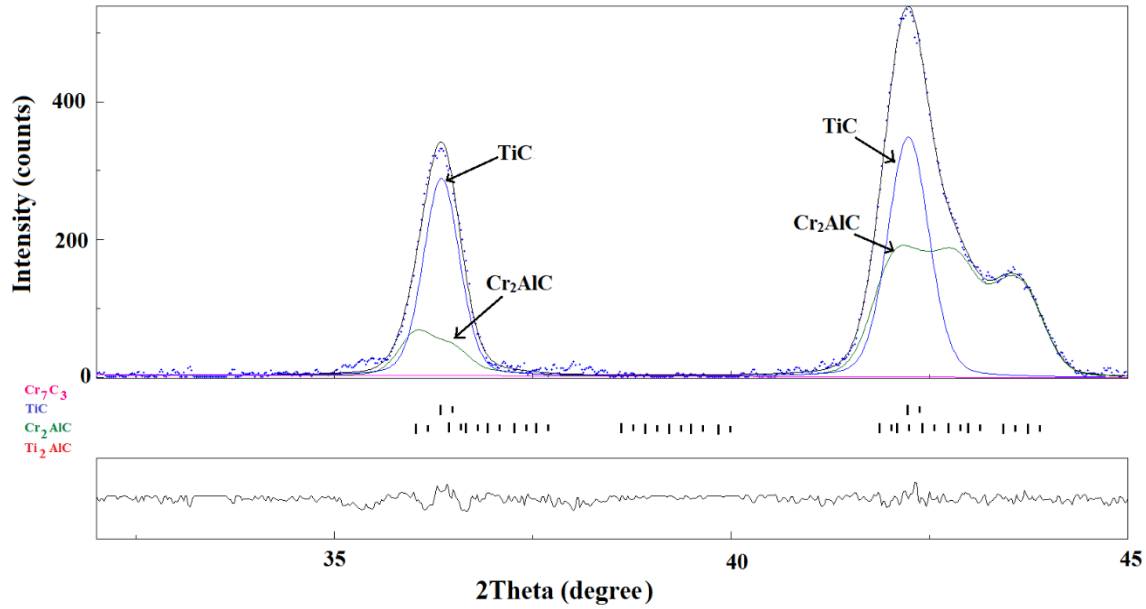
400
200
0
Intensity (counts)
TiC
Cr2AlC
TiC
Cr2AlC
Cr7C3
TiC
Cr2AlC
Ti2AlC
35
40
45
2Theta (degree)

(c)

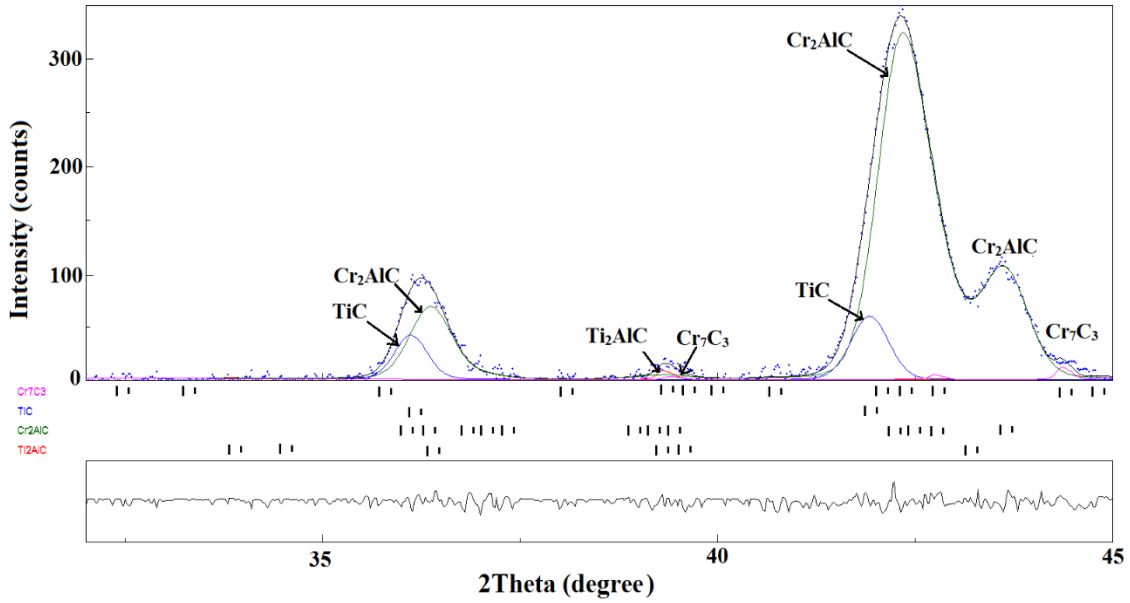

(d)

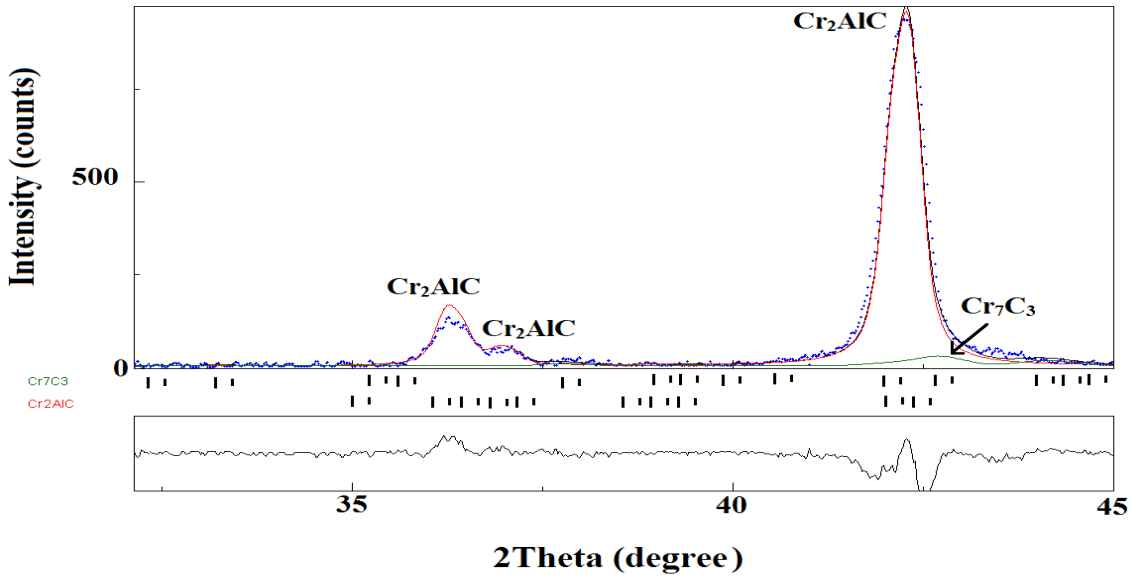

(e)

Fig. 5: High resolution XRD scans of different phases; (a) Ti_2AlC, (b) $(Cr_{0.25}Ti_{0.75})_2AlC$, (c) $(Cr_{0.5}Ti_{0.5})_2AlC$, (d) $(Cr_{0.75}Ti_{0.25})_2AlC$ and (e) Cr_2AlC

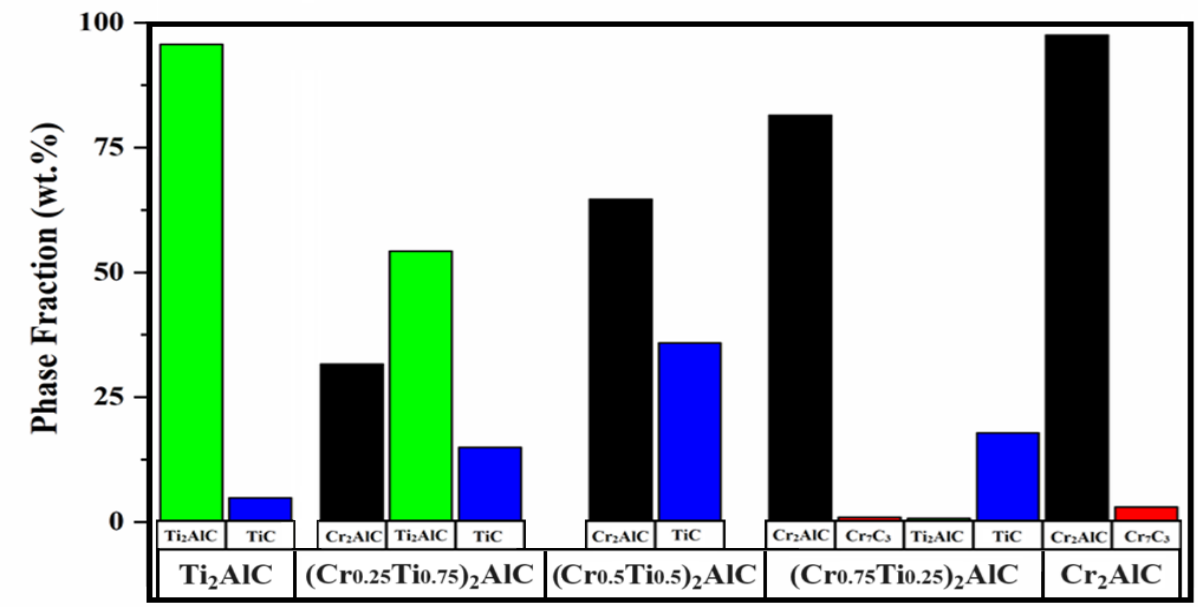

Fig. 6: Phases fraction of the prepared samples

Table 1: Density measurement and Structural data of the SPS-processed samples obtained from Rietveld refinement analysis

Sample			**Ti_2AlC**	**$(Cr_{0.25},Ti_{0.75})_2AlC$**	**$(Cr_{0.5},Ti_{0.5})_2AlC$**	**$(Cr_{0.75},Ti_{0.25})_2AlC$**	**Cr_2AlC**
Density			90	92	95	97.5	96
GOF			1.57	1.43	1.59	1.35	1.24
R_{wp}			9.23	9.14	9.56	8.93	8.32
Ti_2AlC	Weight Percentage		95.40	53.97	-	-	-
	Crystal System		Hexagonal				
	Space Group		$P6_3/mmc$				
	Cell Parameters	α=β	90°	90°	-	-	-
		γ	120°	120°	-	-	-
		a=b (Angstrom)	3.061	3.057	-	-	-
		c (Angstrom)	13.6768	13.589	-	-	-
Cr_2AlC	Weight Percentage		-	31.36	64.36	81.24	97.24
	Crystal System		Hexagonal				
	Space Group		$P6_3/mmc$				
	Cell Parameters	α=β	-	90°	90°	90°	90°
		γ	-	120°	120°	120°	120°
		a=b (Angstrom)	-	2.844	2.849	2.862	2.866
		c (Angstrom)	-	12.401	12.504	12.487	12.791
TiC	Weight Percentage		4.60	14.67	35.64	17.59	-
	Crystal System		Cubic				
	Space Group		Fm-3m				
	Cell Parameters	α=β=γ	90°	90°	90	90	-
		a=b=c	4.328	4.343	4.209	4.320	-
Cr_7C_3	Weight Percentage		-	-	-	1.17	2.76
	Crystal System		Orthorombic				
	Space Group		Pmcn:bca				

	Cell Parameters	α=β=γ	-	-	-	90°	90°
		a	-	-	-	7.010	7.167
		b	-	-	-	12.142	12.648
		c	-	-	-	4.526	4.331

Fig. 7 depicts SEM images with corresponding EDS elemental mapping of the polished surface of Ti_2AlC sample. Regarding to Fig. 7, the specimen surface of specimen shows the presence of Ti, Al and C elements at the same area in the whole surface which can confirm the formation of a ternary compound of Ti-Al-C system. With considering the related XRD pattern in Fig. 4a that shows high content of Ti_2AlC, it can be concluded that the matrix in this sample is Ti_2AlC MAX phase. Moreover, based on EDS elemental analysis, the polished surface of Ti_2AlC sample (gray region) reveals some dark contrast regions which can be considered as TiC (like Ref. [56]) and black regions are porosities. It is worth noting that, in contrast to the Ref. [58], which displays large laminates, our initial sample exhibits small-micro laminates (in the next section higher SEM magnification is presented to see the layers structure). In addition, as depicted in Fig. 7, it is evident that this sample exhibits a high content of pores (the amounts of macro and micropores are high enough to be detected in low magnification SEM image).

The morphology of $(Cr_{0.25}Ti_{0.75})_2AlC$ specimen after polishing process with quantitative EDS analysis is illustrated in Fig. 8. As it can be seen from this image, the areas with the brightest contrast in SEM images has a higher content of Cr element which can confirm the formation of Cr_2AlC MAX phase at these areas (regions “A” and “B”). With the aid of EDS analysis, it can be seen that in the vicinity of bright Cr_2AlC phase, dark gray regions with a high concentration of carbon element have evolved which shows the formation of carbide phases in the interfacial regions (region "D"). As well as the first sample, the polished surface of $(Cr_{0.25}Ti_{0.75})_2AlC$ showed some black dark spot which can be considered as porosity (macro or micro-sized) or particle pulling out. Another gray region of this sample (region “C”) can be correlated to the parent phase (Ti_2AlC).

Fig. 9 reveals SEM images of polished surface of $(Cr_{0.5}Ti_{0.5})_2AlC$ sample. Macro and micro pores are once again clearly detected in this sample. As it can be seen, the bright area of surface of specimens shows the presence of Cr, Al and C elements (the parent phase is Cr_2AlC). Moreover, there are two kinds of gray regions (dark and pale) which seems to be carbide (TiC) and intermetallic (CrAl), respectively. It is worth noting that, in the case of the pale-gray area (blue circles in Fig. 9b), a minor quantity of CrAl intermetallic was identified using EDS, with its content falling below the detection limit of XRD. The existence of the CrAl intermetallic phase is attributed to the higher tendency of Cr to absorb Al compared to Ti. This behavior is a result of the lower Gibbs free energy of formation of Cr-Al compared to Ti-Al compounds (the level of Ti and C is low). The Cr-Al intermetallic phases is detected in the other MAX phase study [25,72].

The introduction of chromium to Ti_2AlC results in a reduction in pore content, particularly notable in the case of $(Cr_{0.75}Ti_{0.25})_2AlC$ due to the absence of macro pores (see Fig. 10a). Different points in Fig. 10a presents various phases (Point E exhibits similarities to point A). The quaternary samples exhibit a composite structure significantly, characterized by different regions/phases with varying contrasts ranging from pale gray to dark gray (compare Fig. 7 and Fig. 11 with Figs. 8a, 9a and 10a). These SEM images indicate a homogeneous distribution of reinforcement phases within the parent/MAX phase. Also, the quantitative EDS point analysis results reveal atomic ratios of (Cr+Ti)/Al that closely approximate 2, as anticipated for $(Cr_xTi_{1-x})_2AlC$. Thus, the SEM-EDS analysis, in conjunction with XRD observations, validates the successful synthesis of a range of distinct composites.

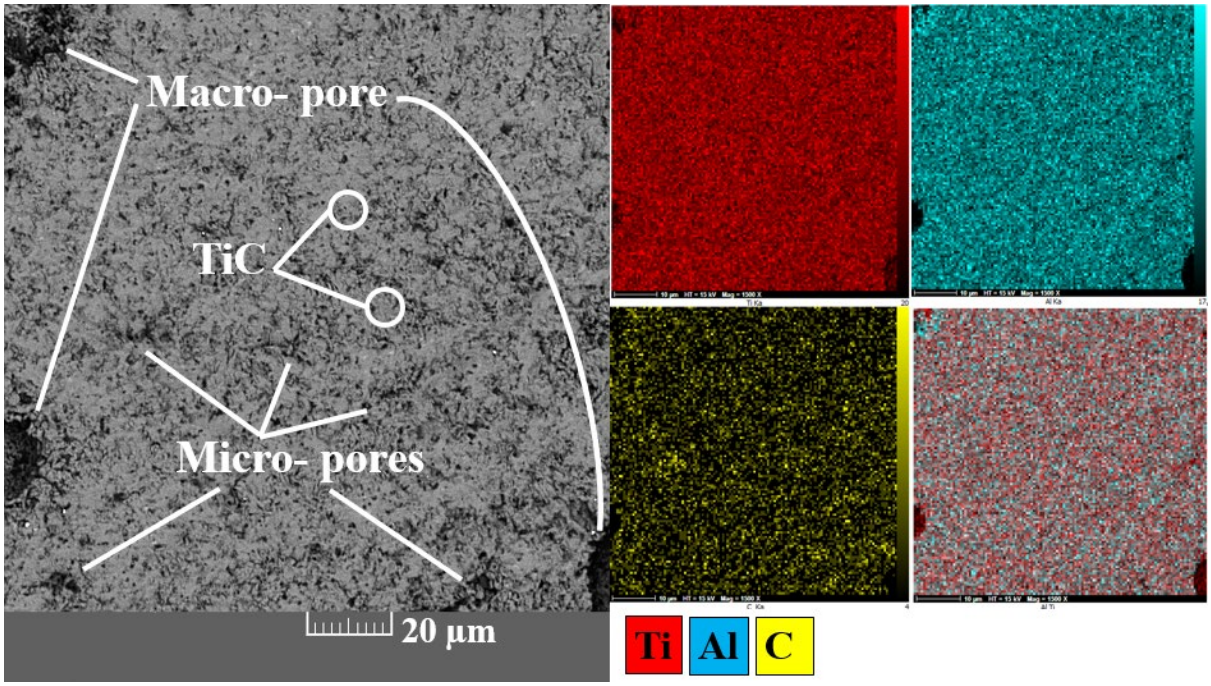

Fig. 7: SEM image with its EDS elemental mapping of the polished surface of Ti_2AlC

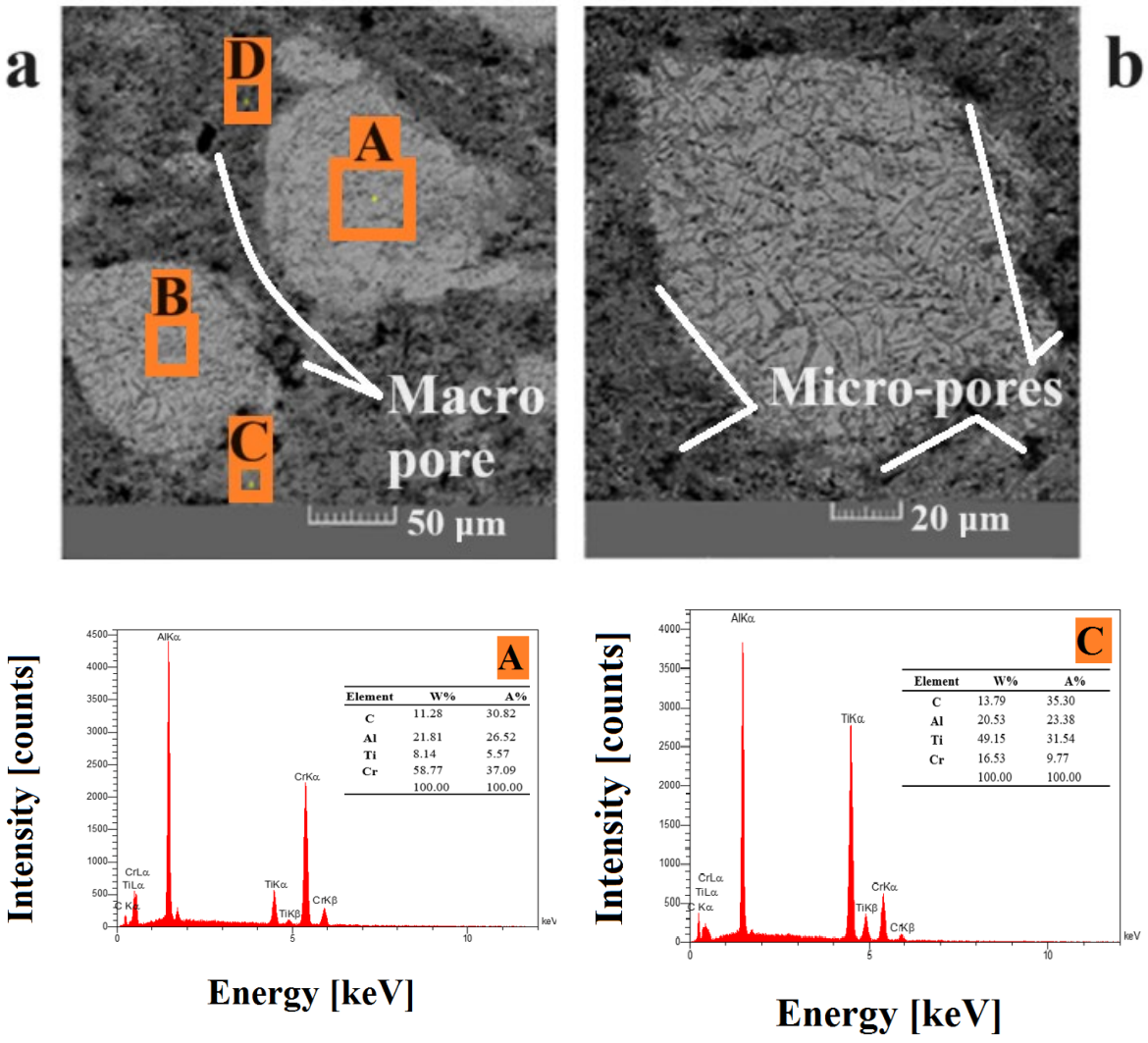

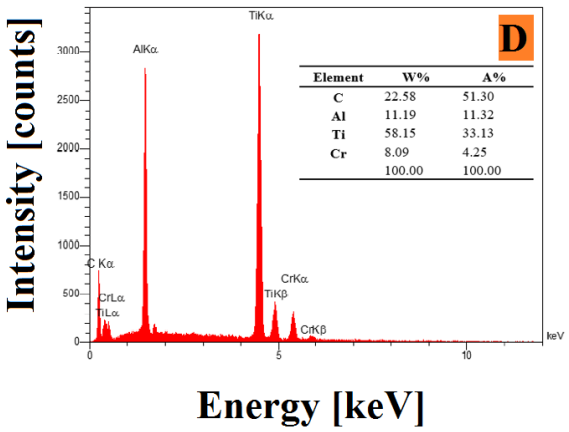

Fig. 8: (a) SEM image of $(Cr_{0.25}Ti_{0.75})_2AlC$; (b) higher magnification of the point B; (c) EDS elemental analysis of the marked points

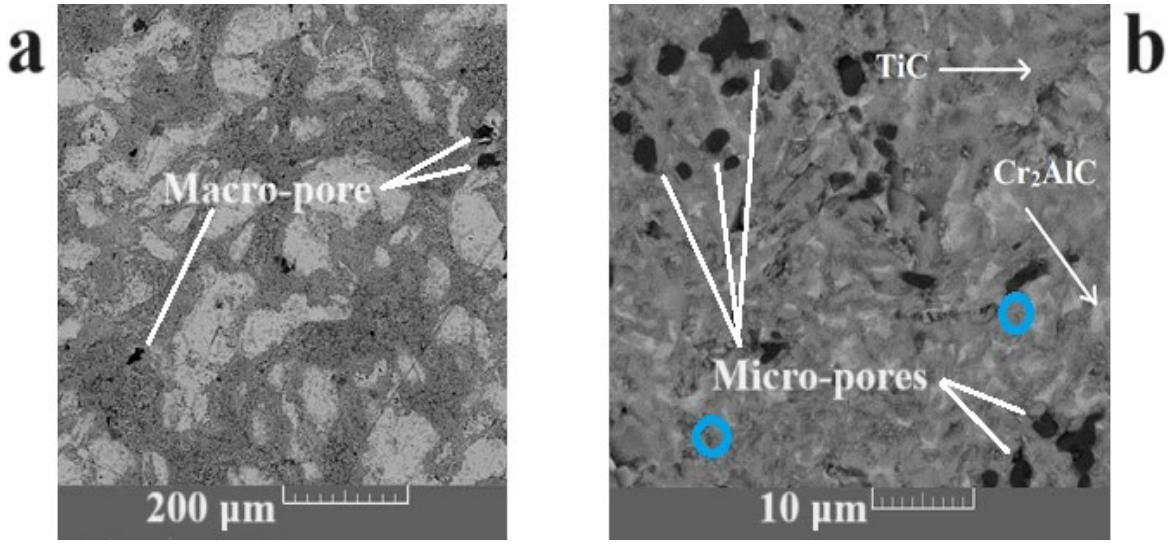

Fig. 9: (a) Low and (b) high magnification of SEM images of the polished surface of $(Cr_{0.5}Ti_{0.5})_2AlC$

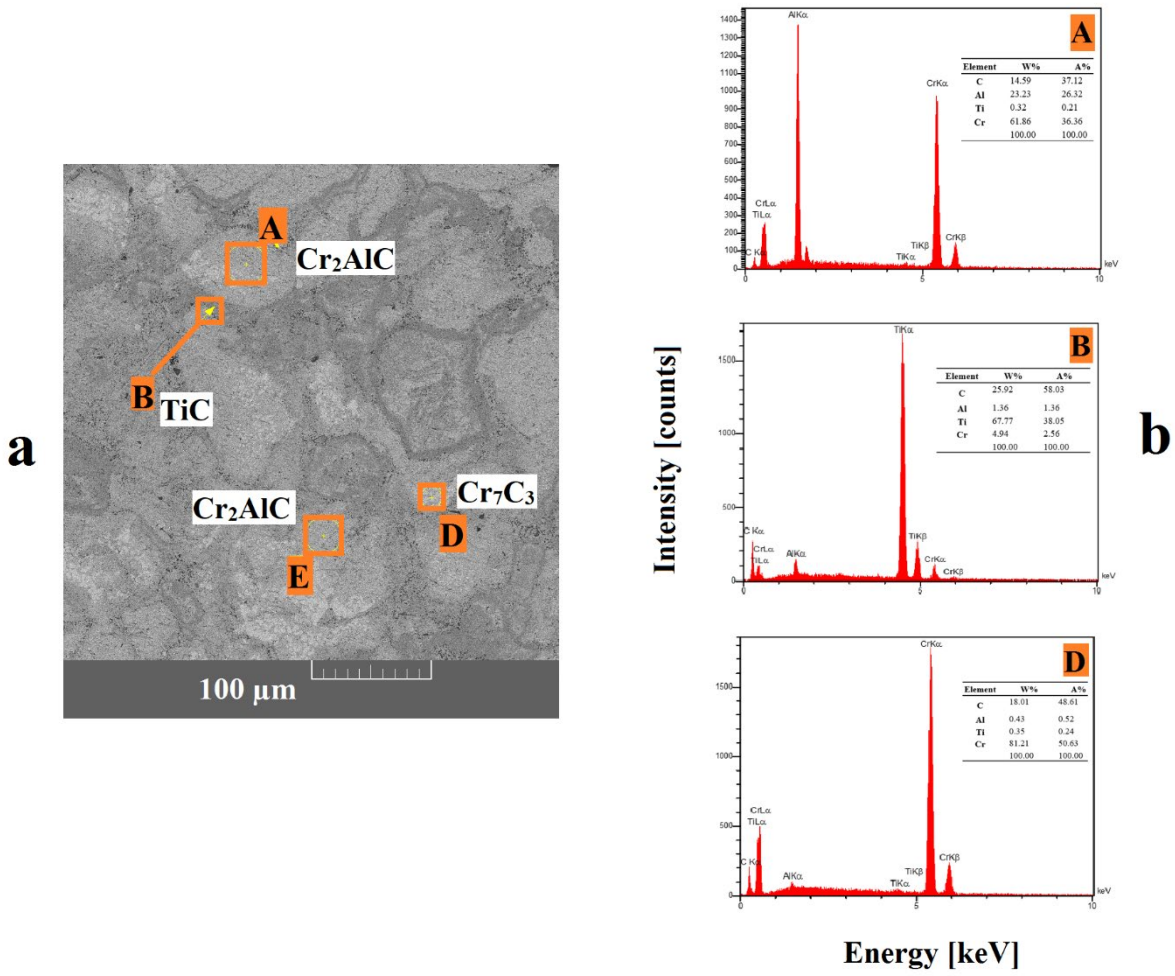

Fig. 10: (a) SEM image, (b) EDS elemental mapping of the polished surface of $(Cr_{0.75}Ti_{0.25})_2AlC$

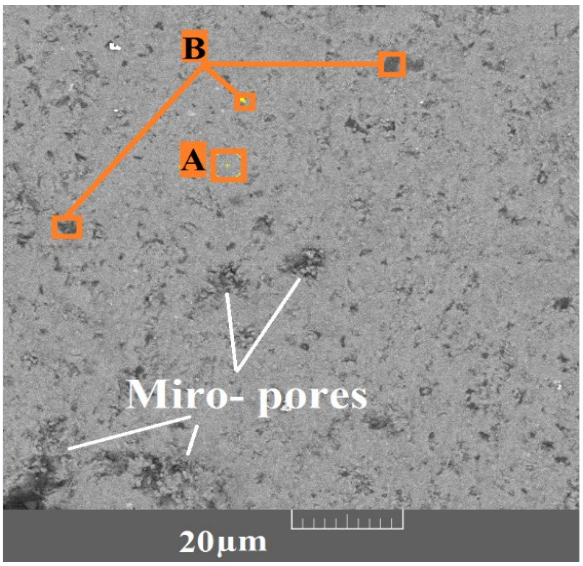

Fig. 11: SEM image of the polished surface of Cr_2AlC sample; A denotes Cr_2AlC and B represents Cr_7C_3 phases.

In all samples, based on EDS data, the impurity content is low (below 3.5 at. %) and the oxygen content is less than 2.5 at. %. Additionally, Cr-rich samples exhibit minimal impurities and oxygen content, typically below 2 atomic percent. Nonetheless, to gain a better understanding of the phases present, it is advisable to conduct complementary tests. Given that carbon is the principal element in the MAX phase systems, Raman spectroscopy can serve as a valuable analytical tool. Fig. 12 illustrates the bond interactions of each sample. It is evident that Ti-rich samples exhibit sharp peaks, while other samples do not show significant peaks. The Raman spectra of Ti_2AlC and $(Cr_{0.25}Ti_{0.75})_2AlC$ reveal the presence of TiO_2 (at 220 cm^{-1}), Al_2O_3 (at 670 cm^{-1}), Cr_2O_3 (at 551cm^{-1} and 745 cm^{-1}), and carbon phases (D and G bands at 1300-1600 cm^{-1}). The locations of the mentioned peaks are consistent with previous research [11,27]. However, as the content of these phases do not meet the criteria for intensity (the level of peak intensity is low) or surface area below the peaks (the noise level is high), further analyses such as crystallite size, vibration characteristics and phase ratios cannot be employed in these cases. Further, it should be mentioned that no distinct and strong peaks were detected in the Cr-rich samples. Additionally, the density of each sample was measured, with the data indicating that the average relative density of Cr_2AlC and $(Cr_{0.75},Ti_{0.25)2}AlC$ is at a maximum (96% and 97.5%, respectively). Conversely, other samples exhibit higher porosity level, as the average relative density of Ti_2AlC, $(Cr_{0.25},Ti_{0.75})_2AlC$ and $(Cr_{0.5},Ti_{0.5})_2AlC$ is 90 %, 92 %, and 95 %, respectively.

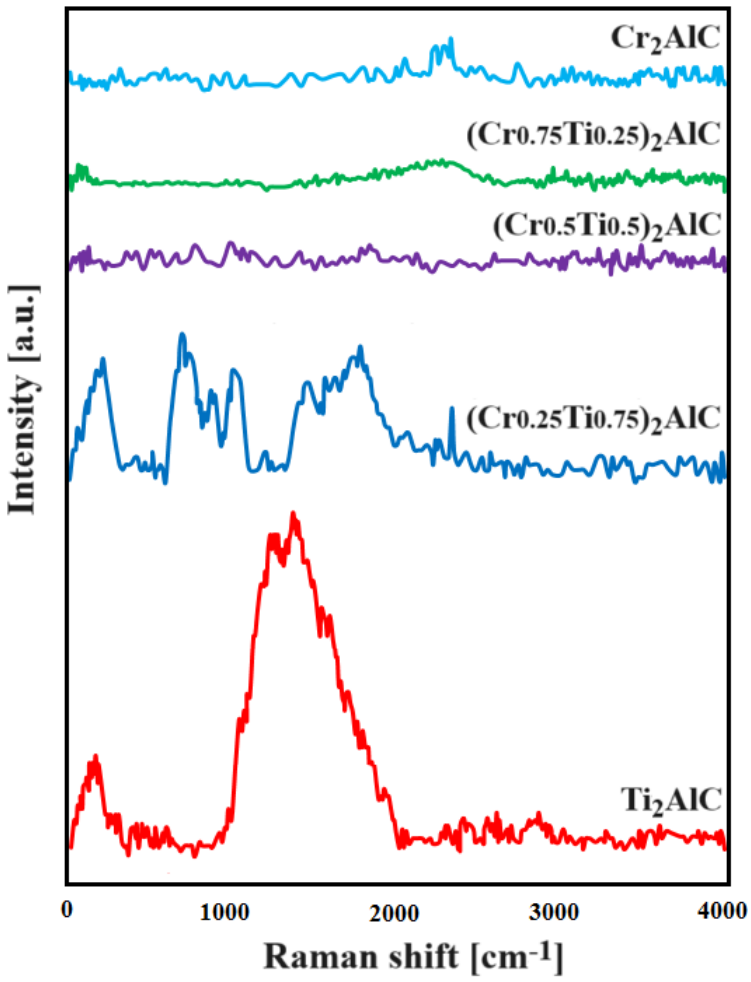

Fig. 12: Raman spectrum of each sample

3.2. Mechanical properties

Table 2 presents the hardness and elastic constants for each sample. Indentation testing determined the hardness and Young's modulus, while the bulk and shear moduli for each sample were derived from previous studies [45,82,83] and the rule of mixture. It is important to acknowledge that the B and G values for each phase are approximate estimates derived from the average of experimental and theoretical values cited in the abovementioned references. This formulation signifies that for each sample B is determined using the formula $\sum w_i \times B_i$, and G is obtained through the equation $\sum w_i \times G_i$, where i represents the phase (Ti_2AlC, Cr_2AlC, TiC, and Cr_7C_3) that holds substantial content in each sample, and w denotes the percentage (it is deduced from Rietveld analysis). Given the low oxygen content in all of the samples, the TiO_2, Al_2O_3 and Cr_2O_3 content is also low and can therefore be neglected in this formulation. The

standard deviation of the hardness measurements was below 0.4 GPa, indicating statistically significant and reliable trends in hardness variation. It should be noted that the load-displacement curves do not exhibit any solid step, pop-in and pop-out. The Young's modulus in the Ti-Al-C system increases monotonously with higher Cr content. However, the trend for hardness, bulk modulus and shear modulus is different. This indicates that with an increase in Cr in Ti-Al-C, H, B and G initially increase, but after a certain percentage, they decrease. This trend can be attributed to composite strengthening (where a higher percentage of carbide phases with higher elastic constants lead to higher strength [84]) and Hall-Petch strengthening (where a lower grain size can result in higher strength [85]). The hardness of $(Cr0.75Ti0.25)_2AlC$ is similar to the fine-grained sample in Ref. [54] but surpasses that of the Ref. [74] due to its higher density, purity and composite structure. However, the other study [73] presents higher hardness (more than 10 GPa) because of lower grain size (either in the case of layer/MAX phase or particle/carbide phase) and nanocomposite structure.

Table 2: Hardness and elastic Modulus for each sample

Sample code/phases	H [GPa]	E [GPa]	B [GPa]	G [GPa]
1/ Ti_2AlC+TiC	5.1	242±5	139.9	119.5
2/ Ti_2AlC+Cr_2AlC+TiC	5.5	254±6	168.1	135.6
3/ Cr_2AlC+TiC	5.9	257±3	211.3	161.3
4/ Cr_2AlC+TiC	6.8	260±3	200.5	153.2
5/ Cr_2AlC+Cr_7C_3	6.3	271±4	196.9	147.5

Fig. 13 displays the fracture images captured from the surface of all samples. Some findings can be made from these images. Firstly, it is evident that the Ti-rich samples (Fig. 13a and Fig. 13b) exhibits a high percentage of voids (small pores). Hence, the initial samples display a brittle fracture pattern attributed to its high porosity and larger grains, facilitating rapid crack coalescence and abrupt failure. Secondly, distinct morphological variations are apparent across different samples, including layered/comb-teeth patterns (like Ref. [75]) and small continuous particle-colony structure. The layered region serves as an indicator of the MAX phase (Ti_2AlC), while particles effectively demonstrates the presence of the carbide phase (TiC). In the case of quaternary samples, Figs. 13b, 13c and 13d, there is particle like shape spots which can be

considered as TiC carbide phase. Moreover, the nano-layered structure depicted in Fig. 13b is a characteristic feature of MAX phases [16]. In the case of the quaternary samples, similar to the previous section, the EDS quantitative analyses from two regions of particle-like shape (indicator of carbide phase) and layered structures (indicator of MAX phase) confirmed the formation of composite structure. Lastly, some areas (particularly at the boundaries of layered materials) display signs of distortion, as depicted in Fig. 13b (red region). This distortion (known as kink bands) can serve as evidence of the plastic deformation capacity of MAX phases (like ref. [27,56]), similar to that of metals. Fig. 13c illustrates a mixed mode of intragranular and intergranular fracture in the $(Cr_{0.5}Ti_{0.5})_2AlC$ sample. This conclusion cab be related to the presence of different phases and voids in this sample (crack paths are at the grain boundaries or in the grains). The incorporation of chromium into Ti_2AlC leads to a decrease in lamellar size. Also, the addition of Cr to Ti_2AlC results in a reduction in brittle and sharp failure. A mixed structure, comprising layers, compactness, particles and ridge lines (like the microstructure presented in references [13,74]), is clearly observed after fracture of sample $(Cr_{0.75}Ti_{0.25})_2AlC$, indicating the presence of multiple fracture mechanisms in this sample (Fig. 13d). As this sample have multiple toughening mechanisms (like composite/particle and Hall-Petch toughening [24,26]), it is predictable to have higher resistance under service conditions (as evidenced by the absence of significant cracks and big voids). It should be noted that Cr-rich samples presents maximum H/E and B/G. Fig. 13e depicts SEM image of the Cr_2AlC sample. This sample exhibits multiple voids, cracks at the boundary (layered Cr_2AlC phase-region "A") and dimples due to brittle fracture. The crack is stopped because of hard carbide phase (region "B"-Cr_7C_3). The Cr_7C_3 phase was identified based on its particle shape and color contrast. All things considered, the composite structure observed in the quaternary samples is a result of distinct phases chemically and diverse morphologies in terms of lamellae and particles.

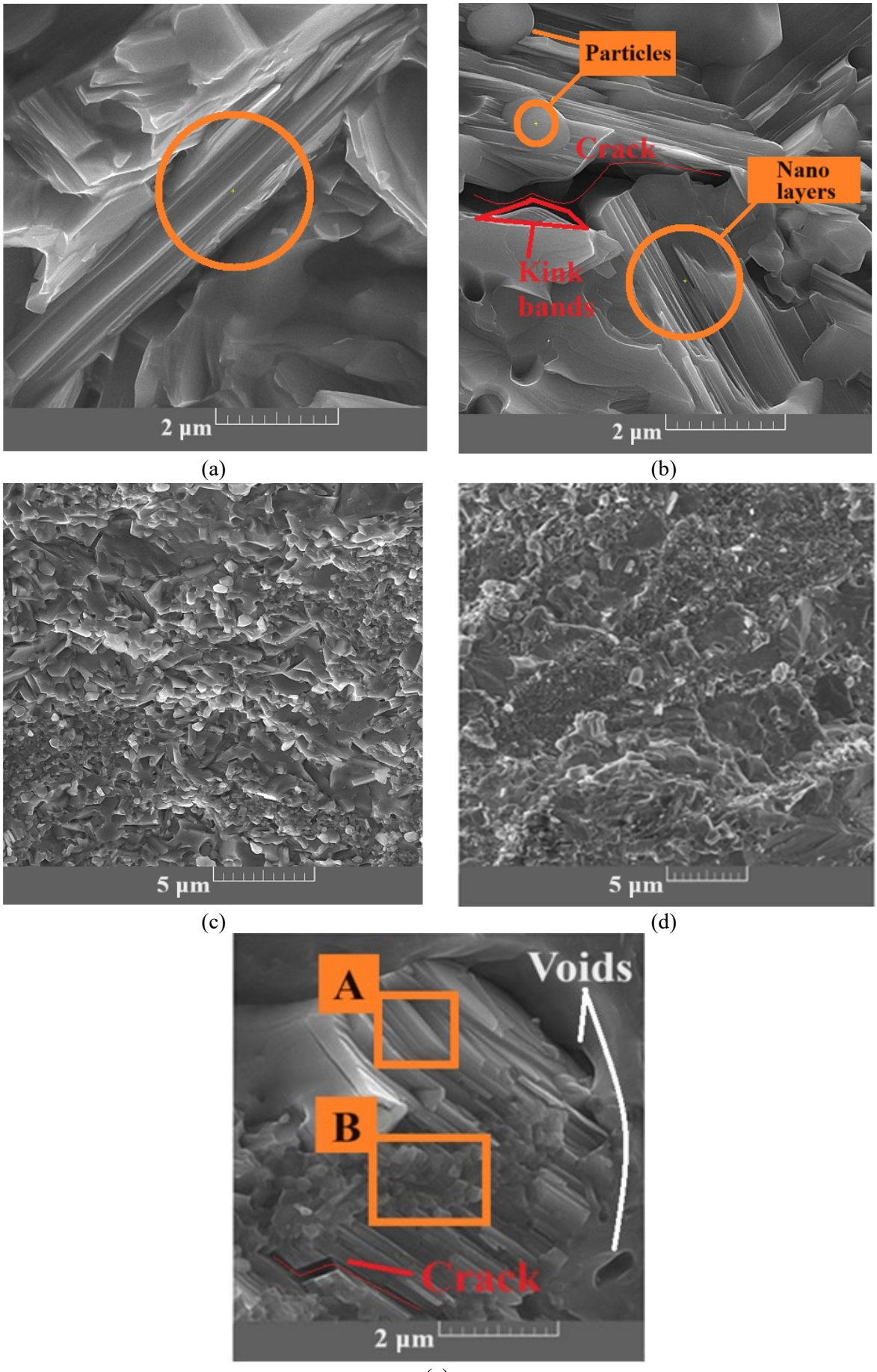

Fig. 13: FESEM images of fracture surface of (a) Ti_2AlC, (b) $(Cr_{0.25}Ti_{0.75})_2AlC$, (c) $(Cr_{0.5}Ti_{0.5})_2AlC$, (d) $(Cr_{0.75}Ti_{0.25})_2AlC$ and (e) Cr_2AlC

Fig. 14 displays the worn surfaces of each sample. By utilizing the equation in section 2 to calculate the wear rate, Fig. 15 illustrates the specific wear rate for each sample. It is observed that Ti_2AlC and $(Cr_{0.25}Ti_{0.75})_2AlC$ exhibit the maximum wear, whereas $(Cr_{0.75}Ti_{0.25})_2AlC$ and Cr_2AlC demonstrate the highest wear resistance (or minimum wear width/rate). The initial sample is anticipated to exhibit high wear due to its pronounced porosity and brittle fracture behavior. In contrast, the $(Cr_{0.75}Ti_{0.25})_2AlC$ sample demonstrates the lowest wear rate owing to its lower porosity, higher purity and mixed fracture mode. Fig. 16 presents the EDS analysis of the marked points in Fig. 14, revealing a minimal tungsten content (nearly 1 at. % in all samples). These results suggest material transfer/adhesion from the pin to the worn surface, indicative of an adhesive wear mechanism. Additionally, the substantial presence of oxygen (26-51 at. %) indicates significant oxidative wear in all samples. Fig. 17 demonstrates the variation of the friction coefficient for each sample. Quaternary system exhibit lower friction (from 0.6 to 0.8) than the ternary samples. Friction coefficients of Ti_2AlC (first sample) and Cr_2AlC (last sample) are more than 0.9. It should be mentioned that the coefficient of friction is determined during the steady state stage and not during the initial running-in period. The Raman spectra presented in Fig. 18 indicate that the $(Cr_xTi_{1-x})_2AlC$ samples contain amorphous carbon and various oxide phases. Comparing the Raman spectra of worn surfaces (Fig. 18) with those of virgin surfaces (Fig. 12) reveals that, similar to Ti-rich samples, the Cr-rich samples also exhibit the presence of amorphous carbon under high-load wear conditions. Apart from the sharp peak of the D and G bands (at 1300-1590 cm^{-1}), minor peaks corresponding to TiO_2, Al_2O_3, and Cr_2O_3 are present in the Raman spectra of the $(Cr0.25Ti0.75)_2AlC$, $(Cr_{0.75}Ti_{0.25})_2AlC$ and $(Cr_{0.5}Ti_{0.5})_2AlC$, respectively. Lower friction coefficients of quaternary samples can be attributed to the synergistic effects of the presence of amorphous carbon (due to graphitization under loading [85]) and oxide tribo-layers (due to bearing effect under sliding [12]), which can facilitate sliding and lubrication. Therefore, the quaternary samples exhibit self-lubricating feature. The lubricating effect of the graphitic phase and the protective effect

of oxide tribo-films (situated on the wear tracks of the MAX phase materials) have been robustly validated [27], particularly in the studies conducted by Magnus et al. [11,58].

Under high loads and ambient air (as compression-tension, oxidation and fatigue phenomena are highly likely to happen [86]) wear is a complicated phenomenon. Usually previous studies relate hardness to the wear performance of materials, however elastic constants should be regarded at the same time. To address this issue, Fig. 19a clearly shows the relationship of the hardness to Young's Modulus ratio to the specific wear rate and Fig. 19b shows the relationship of the bulk to shear modulus ratio (Pugh ratio) to the specific wear rate. These parameters serve as indicators of ductility-brittleness [87] and deformation in relation to the yielding [84] of materials. The trend lines of both curves are reliable because the R^2 values are higher than 0.91. Fig. 19 illustrates that maximum H/E and B/G values can result in minimized wear. Elastic constants are associated with the bond type and chemistry of materials [45,82]. Hence, based on these trends, it is recommended to have higher hardness and bulk modulus for improved wear performance, as these properties contribute to higher strength that resists material cutting and fracturing. Additionally, it is advantageous to have lower Young's modulus and shear modulus to facilitate better lubricating and sliding conditions for a tribo-pair system. However, in order to elucidate the mechanical properties of each sample, it is beneficial to also consider another aspect: porosity and defect/impurities content. Hence, with everything considered, $(Cr_{0.75}Ti_{0.25})_2AlC$ and Cr_2AlC demonstrate maximum hardness and wear resistance (minimum wear rate) due to their high density and significant content of Cr_7C_3 and Cr_2AlC, while the content of oxygen and impurities is negligible.

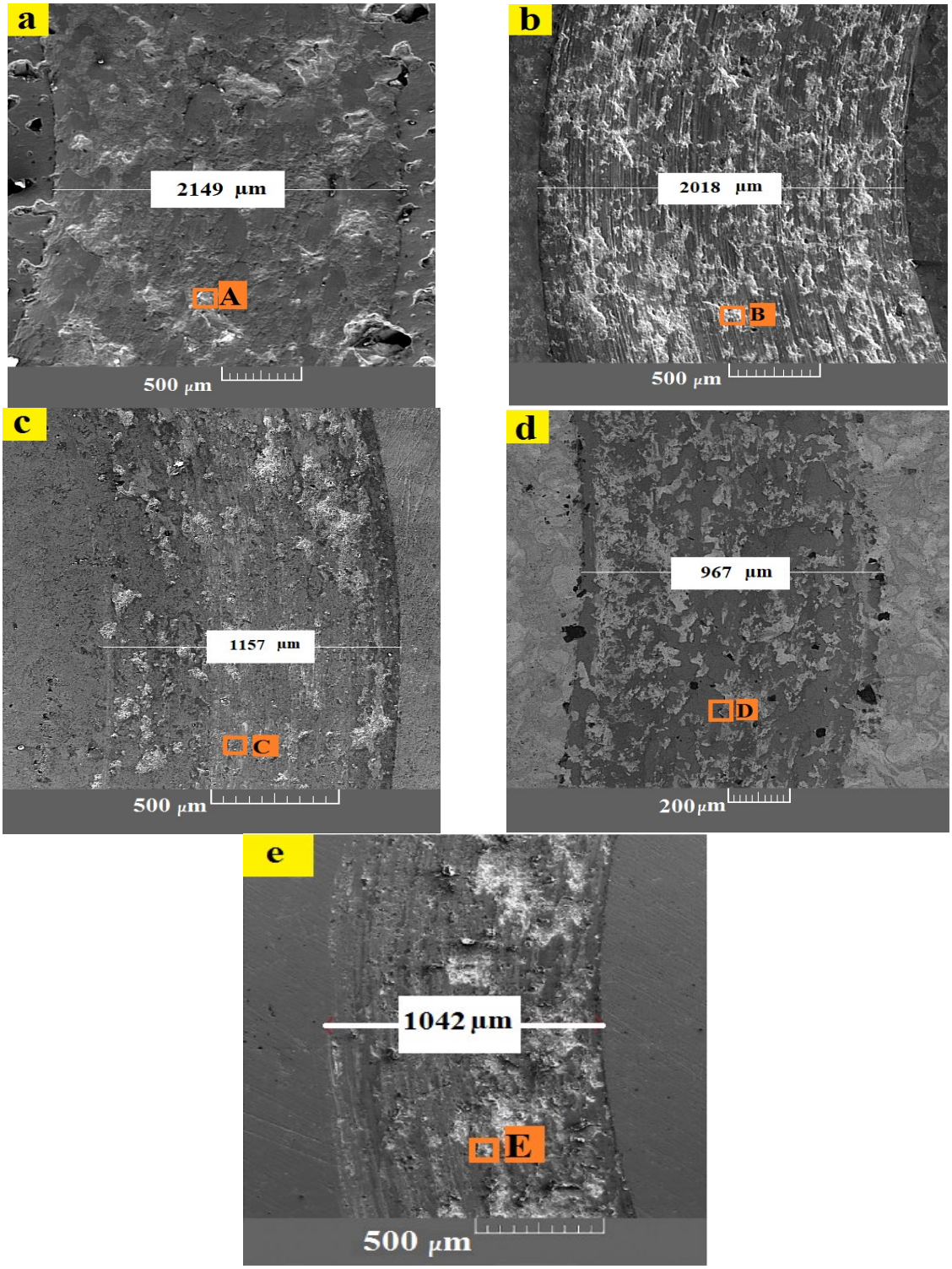

Fig. 14: Low magnification SEM micrographs related to the worn samples; (a) Ti_2AlC, (b) $(Cr_{0.25}Ti_{0.75})_2AlC$, (c) $(Cr_{0.5}Ti_{0.5})_2AlC$, (d) $(Cr_{0.75}Ti_{0.25})_2AlC$ and (e) Cr_2AlC

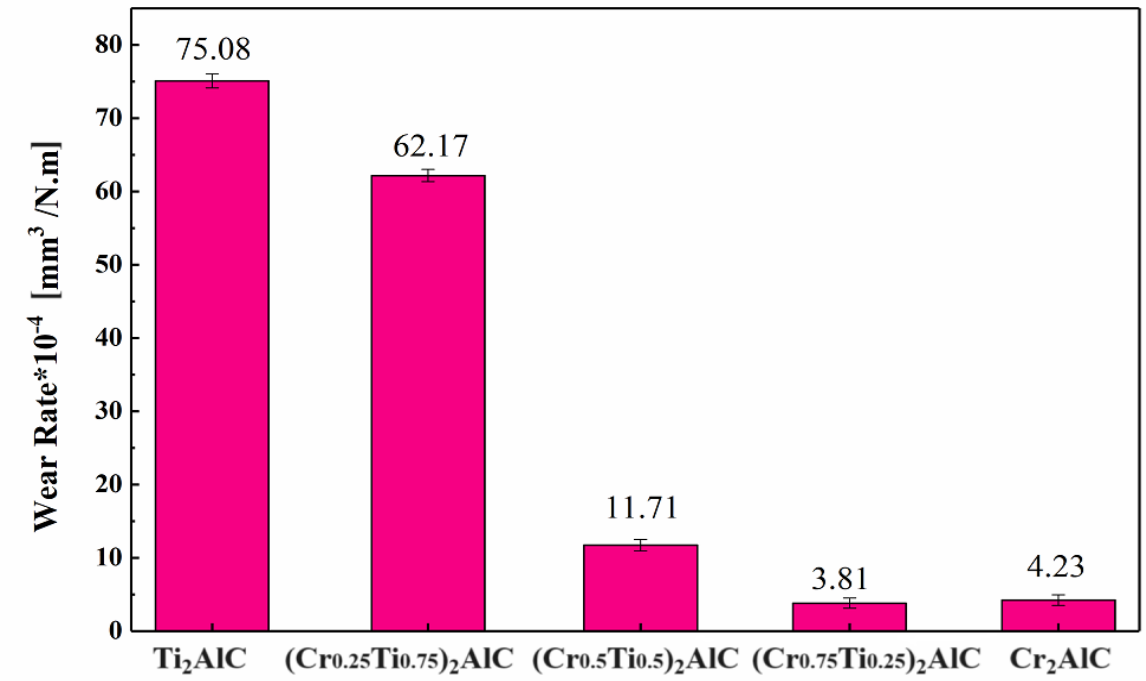

Fig. 15: Specific wear rate for each sample

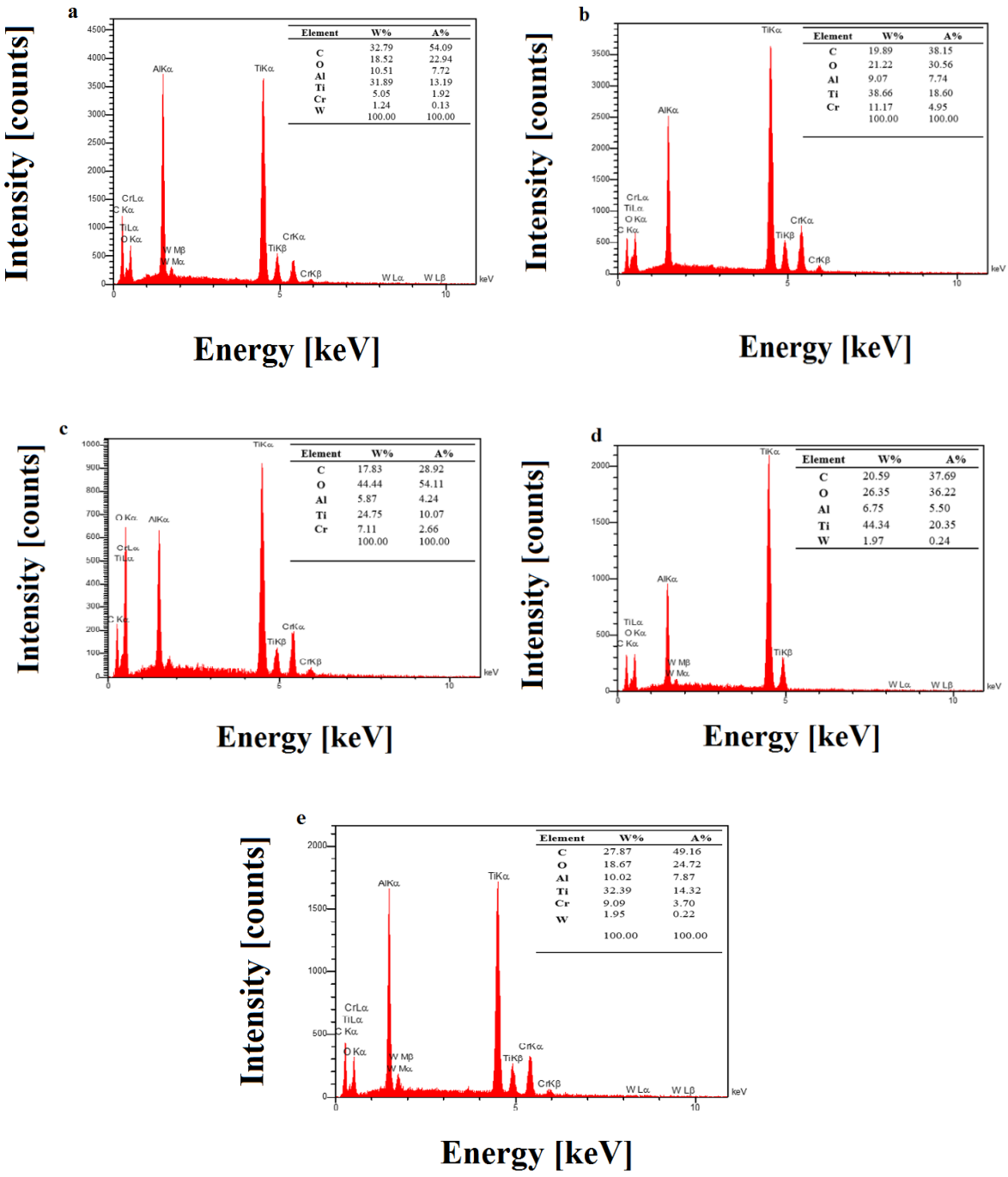

Fig. 16: EDS-point analysis from the wear track of each sample based on Fig. 14; (a) point A, (b) point B, (c) point C, (d) point D, and (e) point E

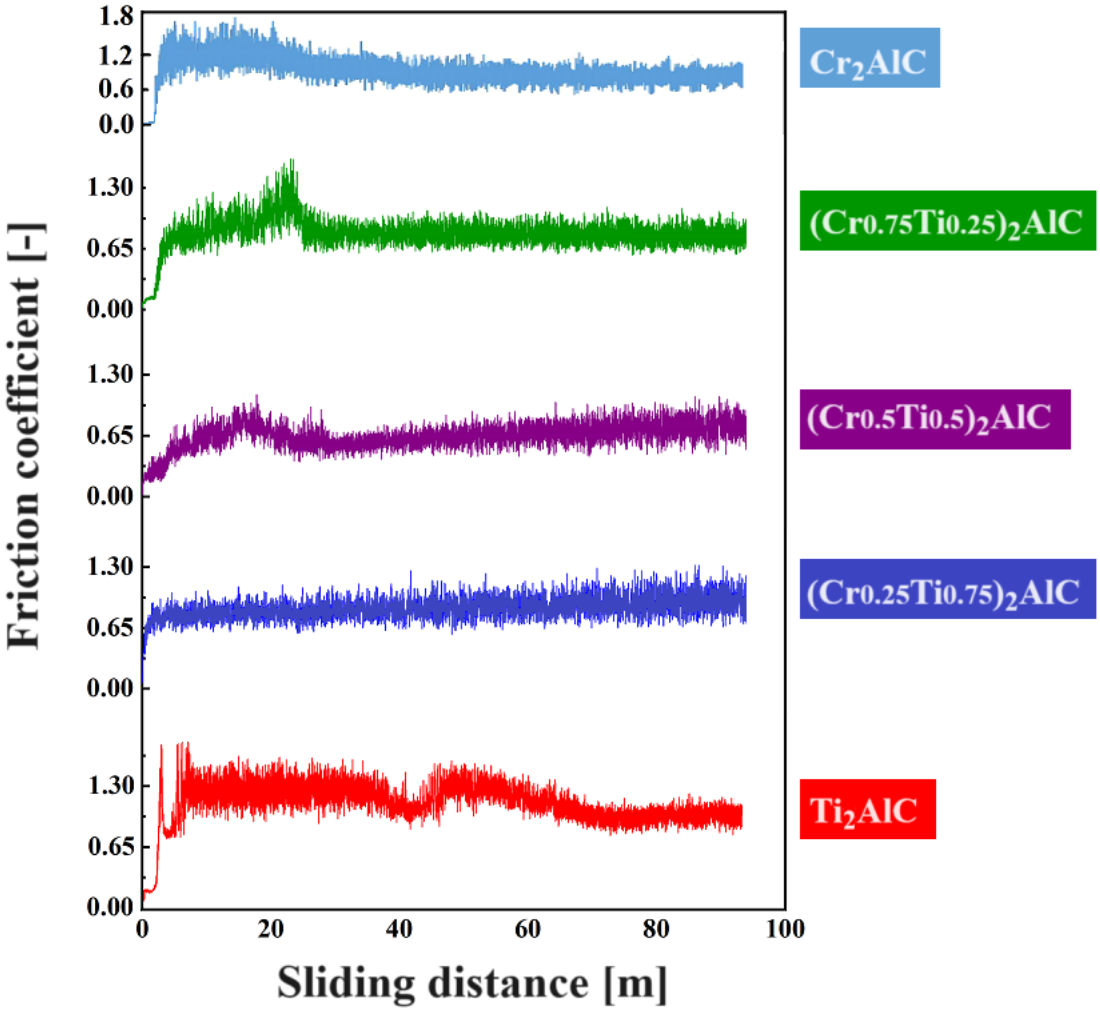

Fig. 17: Variation of coefficient of friction for each sample

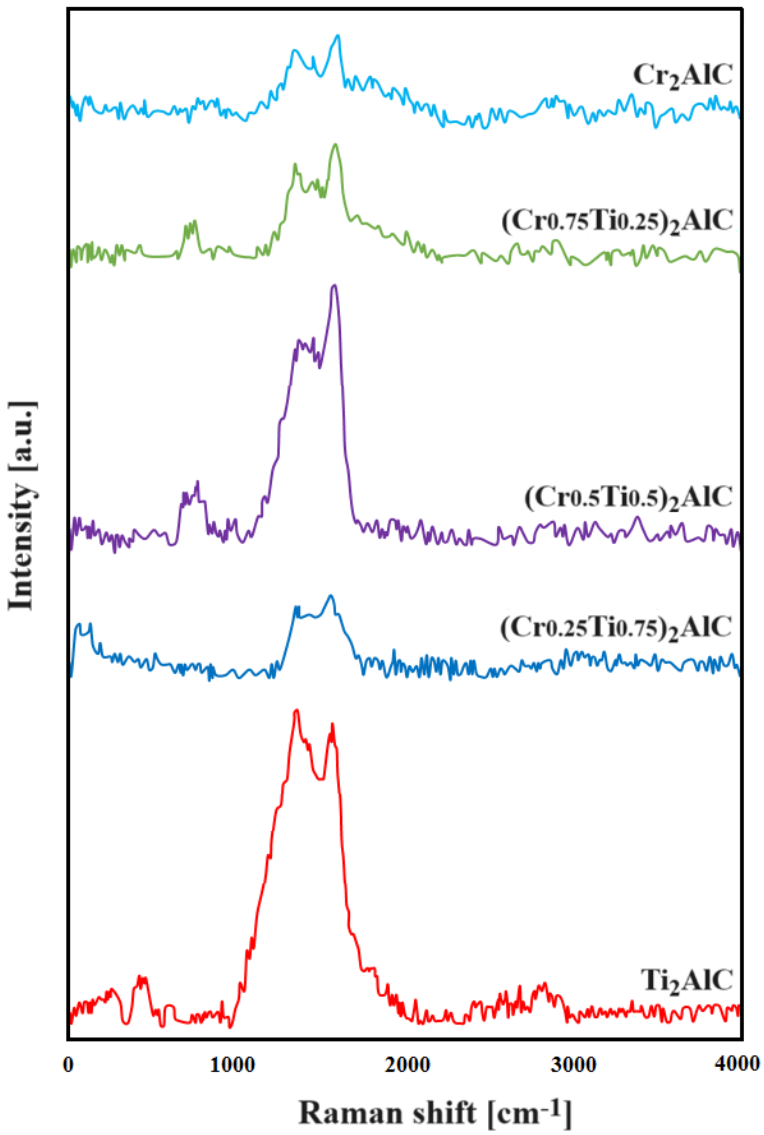

Fig. 18: Raman spectrum of each sample after sliding test

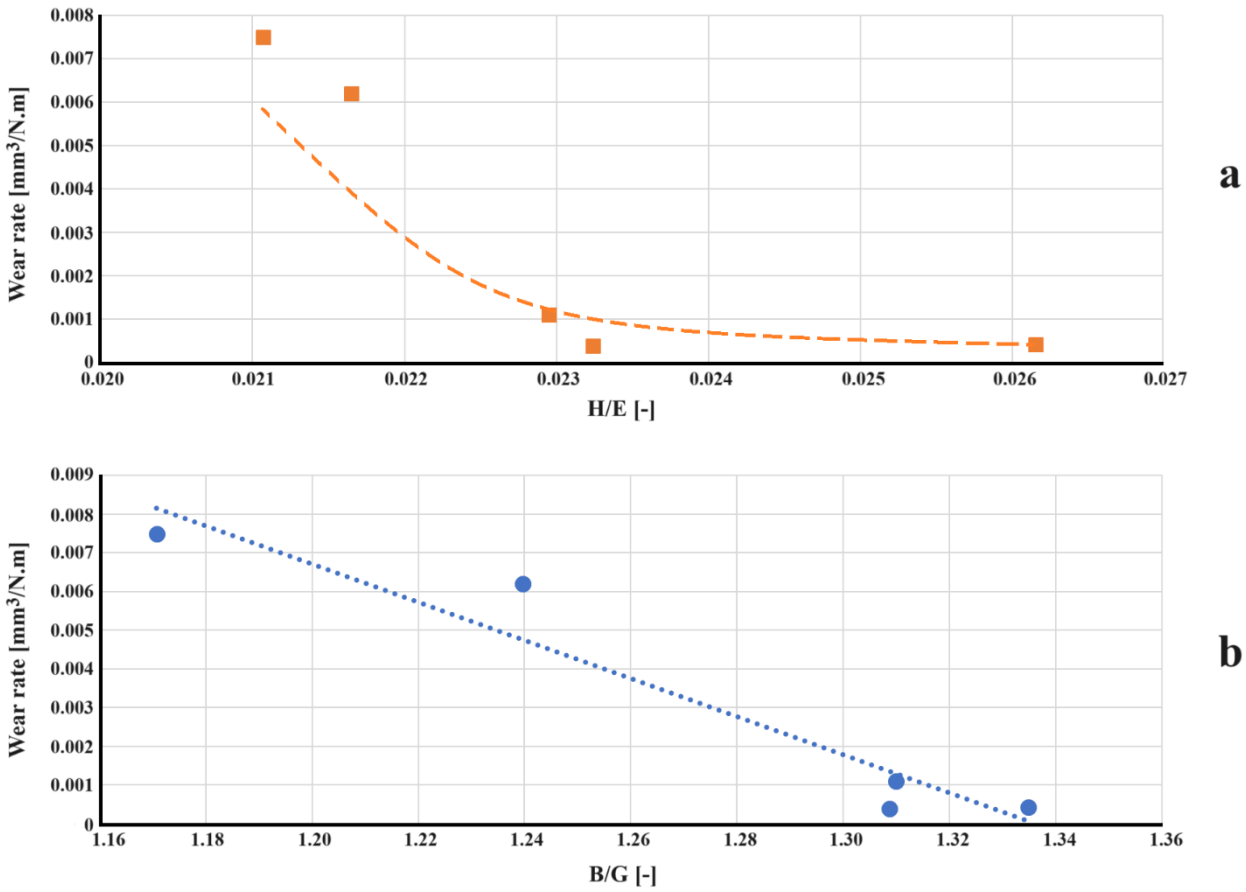

Fig. 19: Effect of (a) H/E and (b) B/G on wear rate of each sample

4. Conclusion

Using ball-milling and spark plasma sintering quaternary system consists of Ti-Cr-Al-C is successfully produced. In addition, various characterization, mechanical and tribological tests are presented in this paper. Therefore, the main outputs of the study can be summarized as follows:

1. Porosity and impurities are minimized in Cr-rich samples, with porosity in Cr_2AlC and $(Cr_{0.75}Ti_{0.25})_2AlC$ being less than 4% and impurities content less than 2 at. %.
2. XRD and SEM results of the samples show composite structure (MAX phase as the parent phase and carbide phase as the reinforcement phase). Based on the analysis of the fracture surfaces, it can be inferred that the addition of chromium can lead to a change in the failure mode. In Ti-rich samples, the fracture exhibits a brittle behavior

characterized by comb teeth and various types of voids, both micro and macro in nature. Conversely, in the case of $(Cr_{0.5}Ti_{0.5})_2AlC$ and $(Cr_{0.75}Ti_{0.25})_2AlC$, the fracture mode is observed to be mixed, featuring ridge lines, compactness and fine grains.

3. The friction coefficients of quaternary samples are lower than ternary system due to the synergistic effect of the existence of graphite and oxide-tribo-layer, which were confirmed to be in the wear track using Raman spectroscopy.
4. Wear resistance of the samples is directly dependent on the mechanical parameters (H/E and B/G), with Cr-rich samples exhibiting maximum values of these parameters and minimum wear rate.

Declaration of Competing Interest

None.

References

[1] A. Zhou, "Methods of MAX-phase synthesis and densification–II", Adv. Sci. Technol. Mn+ 1axn Phases (2012) 21–46. DOI:10.1533/9780857096012.21

[2] K. Xiong, Z. Sun, S. Zhang, Y. Wang, W. Li, L. You, L. Yang, L. Guo, Y. Mao, "A comparative study the structural, mechanical, and electronic properties of medium-entropy MAX phase $(TiZrHf)_2SC$ with Ti_2SC, Zr_2SC, Hf_2SC via first principles", J. Mater. Res. Tech. 19 (2022) 2717-2729. DOI: 10.1016/j.jmrt.2022.06.040

[3] E. Drouelle, V. Brunet, J. Cormier, P. Villechaise, P. Sallot, F. Naimi, F. Bernard, S. Dubois, "Oxidation resistance of Ti_3AlC_2 and $Ti_3Al_{0.8}Sn_{0.2}C_2$ MAX phases: A comparison", J. Am. Ceram. Soc. 103 (2020) 1270‑1280. DOI:10.1111/jace.16780

[4] D. B. Lee, T. D. Nguyen, S. W. Park, "High Temperature Oxidation of a Nanolayer Laminated $(Cr0.95Ti0.05)_2AlC$ Compound in Air", J. Nano sci. Nano technol. 10 (2010) 319–324. DOI:10.1166/jnn.2010.1522

[5] A. Lashkari, A. Ostovari Moghaddam, M. Naseri, A. Shokuhfar, "Synthesis and characterization of high

entropy carbide-MAX two-phase composites", J. Mater. Res. Tech. 24 (2023) 5024-5031. DOI:10.1016/j.jmrt.2023.04.125

[6] W. Ding, H. Chen, Y. Bao, L. Chu, Q. Feng, C. Hu, "Ultra-fast thermal shock behavior of Cr_2AlC ceramics up to 1300°C", Ceram. Inter. In Press. https://doi.org/10.1016/j.ceramint.2024.01.110

[7] T. Lapauw, A.K. Swarnakar, K. Lambrinou, B. Tunca, J. Vleugels, "Nanolaminated ternary carbide (MAX phase) materials for high temperature applications", Int. J. Ref. Met. Hard Mater. 72 (2018) 51-55. DOI:10.1016/j.ijrmhm.2017.11.038

[8] M. Nadeem, M. Haseeb, A.Hussain, A. Javed, M. Amir Rafiq, M. Ramzan, M.N. Rasul, M. Azhar Khan, "Structural stability, electronic structure, mechanical and optical properties of MAX phase ternary Mo_2Ga_2C, Mo_2GaC and Mo_3GaC_2 carbides", J. Mater. Res. Tech. 14 (2021) 521-532. DOI:10.1016/j.jmrt.2021.06.079

[9] K. Lambrinou, T. Lapauw, B. Tunca, J. Vleugels, "MAX Phase Materials for Nuclear Applications", Book Series:Ceramic Engineering and Science Proceedings-Chapter 21, J. Am. Ceram. Soc. (2017). DOI: 10.1002/9781119321811.ch21

[10] E. Ghasali, M. R. Derakhshandeh, Y. Orooji, M. Alizadeh, T. Ebadzadeh, "Effects of 211 and 413 ordering on the corrosion behavior of V-Al-C MAX phases prepared by spark plasma sintering", J. Euro. Ceram. Soc. 41 (2021) 4774–4787. DOI:10.1016/j.jeurceramsoc.2021.03.001

[11] C. Magnus, W. M. Rainforth, "Spark plasma sintering (SPS) synthesis and tribological behaviour of MAX phase composite of the family $Ti_{n+1}SiC_n$ (n= 2)", Wear 438–439 (2019) 203062. DOI:10.1016/j.wear.2019.203062

[12] L. Cai, J. Li, B. Luo, J. Yang, N. He, J. Jia, "Self-lubricating effect of solid solution elements on tribological performance of Ti_3AlC_2 over a wide temperature range", J. Am. Ceram. Soc. (2024) 1‑14. DOI: 10.1111/jace.19662

[13] R. Ali, P. Song, M. Khan, S. Ali, M. R. Kamli, J. S.M. Sabir, T. Huang, A. Deifalla, Shakeel, J. Lu, "Tribological and oxidation resistance performance of Ti2AlC MAX-phase generated by reactive spark plasma sintering", J. Mater. Res. Tech. 26 (2023) 8309-8326. https://doi.org/10.1016/j.jmrt.2023.09.110

[14] S. Li, G. Song, K. Kwakernaak, S. van der Zwaag, W. G. Sloof, "Multiple crack healing of a Ti2AlC ceramic", J. Euro. Ceram. Soc. 32 (2012) 1813–1820. DOI:10.1016/j.jeurceramsoc.2012.01.017

[15] W. Yu, S. Li, W. G. Sloof, "Microstructure and mechanical properties of a $Cr_2Al(Si)C$ solid solution",

Mater. Sci. Eng. A 527 (2010) 5997–6001. DOI:10.1016/j.msea.2010.05.093

[16] J. Gonzalez-Julian, "Processing of MAX phases: From synthesis to applications", J. Am. Ceram. Soc. 104 (2021) 659‑690. DOI: 10.1111/jace.17544

[17] M. Haftani, M.S. Heydari, H.R. Baharvandi, N. Ehsani, "Studying the oxidation of Ti_2AlC MAX phase in atmosphere: A review", Int. J. Ref. Met. Hard Mater. 61 (2016) 51–60. DOI:10.1016/j.ijrmhm.2016.07.006

[18] N. Atazadeh, M.S. Heydari, H.R. Baharvandi, N. Ehsani, "Reviewing the effects of different additives on the synthesis of the Ti_3SiC_2 MAX phase by mechanical alloying technique", Int. J. Refract. Met. Hard Mater. 61 (2016) 67–78. DOI:10.1016/j.ijrmhm.2016.08.003

[19] P. Eklund, M. Beckers, U. Jansson, H. Högberg, L. Hultman, "The $M_{n+1}AX_n$ phases: Materials science and thin-film processing", Thin Solid Films. 518 (2010) 1851–1878. DOI:10.1016/j.tsf.2009.07.184

[20] Y. Medkour, A. Roumili, D. Maouche, L. Louail, "Electrical properties of MAX phases, Advances in Science and Technology of $M_{n+1}AX_n$ Phases", (2012). DOI:10.1533/9780857096012.159

[21] W. Jeitschko, H. Nowotny, F. Benesovsky, "Ti_2AlN eine stickstoffhaltige H-Phase", Monatshefte für Chemie und verwandte Teile anderer Wissenschaften 94 (1963) 1198–1200. DOI:10.1007/BF00905710

[22] W. Jeitschko, H. Nowotny, F. Benesovsky, "Carbides of formula T_2MC", Journal of the Less Common Metals 7 (1964) 133-138. DOI:10.1016/0022-5088(64)90055-4

[23] M. W. Barsoum, T. El-Raghy, "Synthesis and Characterization of a Remarkable Ceramic: Ti_3SiC_2", J. Am. Ceram. Soc. 79 (1996) 1953-1956. DOI:10.1111/j.1151-2916.1996.tb08018.x

[24] X. Chen, G. Bei, "Toughening Mechanisms in Nanolayered MAX Phase Ceramics—A Review", Materials 10 (2017) 366. DOI:10.3390/ma10040366

[25] J. Liu, X. Zuo, Z. Wang, L. Wang, X. Wu, P. Ke , A. Wang, "Fabrication and mechanical properties of high purity of Cr2AlC coatings by adjustable Al contents", J. Alloys Compd. 753 (2018) 11-17. DOI:10.1016/j.jallcom.2018.04.100

[26] J. Lyu, E. B. Kashkarov, N. Travitzky, M. S. Syrtanov, A. M. Lider, "Sintering of MAX-phase materials by spark plasma and other methods", J. Mater. Sci. 56 (2021) 1980. DOI:10.1007/s10853-020-05359-y

[27] L. Fu, W. Xia, "MAX Phases as Nanolaminate Materials: Chemical Composition, Microstructure, Synthesis, Properties, and Applications", Adv. Eng. Mater. 23 (2021) 2001191. DOI:

10.1002/adem.202001191

[28] M.W. Barsoum, Physical properties of the MAX phases, "Encyclopedia of Materials: Science and Technology", 1 (2006) 1–11. https://doi.org/10.1016/B0-08-043152-6/02058-1

[29] M.W. Barsoum, T. El-Raghy, "The MAX phases: Unique new carbide and nitride materials: Ternary ceramics turn out to be surprisingly soft and machinable, yet also heat-tolerant, strong and lightweight", Am. Sci. 89 (2001) 334–343. https://www.jstor.org/stable/27857502

[30] E. Ghasali, Y. Orooji, H.N. Germi, "Investigation on in-situ formed Al_3V-Al-VC nano composite through conventional, microwave and spark plasma sintering", Heliyon. 5 (2019) e01754. DOI:10.1016/j.heliyon.2019.e01754

[31] D. Aydogmus, O. Duygulu, F. Cinar Sahin, “In-situ spark plasma sintering behavior of La_2O_3-Y_2O_3 co-doped AlON ceramics: An attempt to prevent carbon contamination”, J. Mater. Res. Tech. 27 (2023) 2323-2335. DOI:10.1016/j.jmrt.2023.10.047

[32] Y. Wang, G. Rong, T. Ma, Z. Chen, X. Zhang, D. Zhu, H. Fang, R. Chen, “In-situ synthesized a dual-scale Ti2AlC reinforced TiAl composites with superior mechanical properties”, J. Mater. Res. Tech. 28 (2024) 1667–1678. DOI:10.1016/j.jmrt.2023.12.092

[33] S.A.A. Alem, R. Latifi, S. Angizi, F. Hassanaghaei, M. Aghaahmadi, E. Ghasali, M. Rajabi, "Microwave sintering of ceramic reinforced metal matrix composites and their properties: a review", Mater. Manuf. Process. 35 (2020) 303–327. DOI:10.1080/10426914.2020.1718698

[34] E. Ghasali, K. Baghchesaraee, Y. Orooji, "Study of the potential effect of spark plasma sintering on the preparation of complex FGM/laminated WC-based cermet", Int. J. Refract. Met. Hard Mater. (2020) 105328. DOI:10.1016/j.ijrmhm.2020.105328

[35] E. Ghasali, A. Bordbar-Khiabani, M. Alizadeh, M. Mozafari, M. Niazmand, H. Kazemzadeh, T. Ebadzadeh, "Corrosion behavior and in-vitro bioactivity of porous Mg/Al2O3 and Mg/Si3N4 metal matrix composites fabricated using microwave sintering process", Mater. Chem. Phys. 225 (2019) 331–339. DOI:10.1016/J.MATCHEMPHYS.2019.01.007

[36] S.A.A. Alem, R. Latifi, S. Angizi, N. Mohamadbeigi, M. Rajabi, E. Ghasali, Y. Orooji, "Development of Metal Matrix Composites and Nanocomposites Via Double-Pressing Double-Sintering (DPDS) Method", Mater. Today Commun. 25 (2020) 101245. DOI:10.1016/j.mtcomm.2020.101245

[37] A. Shamsipoor, M. Farvizi, M. Razavi, A. Keyvani, "Influences of processing parameters on the

microstructure and wear performance of Cr_2AlC MAX phase prepared by spark plasma sintering method", J. Alloys Compd. 815 (2020) 152345. DOI:10.1016/j.jallcom.2019.152345

[38] A. Shamsipoor, M. Farvizi, M. Razavi, A. Keyvani, B. Mousavi, W. Pan, "High-temperature oxidation behavior in YSZ coated Cr_2AlC and CoNiCrAlY substrates", Surf. Coat. Technol. 401 (2020) 126239. DOI:10.1016/j.surfcoat.2020.126239

[39] M. Dahlqvist, B. Alling, J. Rosén, "Stability trends of MAX phases from first principles", PHYS. REV. B 81 (2010) 220102. DOI: 10.1103/PhysRevB.81.220102

[40] I. Salama, T. El-Raghy, M.W. Barsoum, "Synthesis and mechanical properties of Nb2AlC and $(Ti,Nb)_2AlC$", J. Alloys Compd. 347 (2002) 271–278. DOI:10.1016/S0925-8388(02)00756-9

[41] D.J. Tallman, B. Anasori, M.W. Barsoum, "A critical review of the oxidation of Ti2AlC, Ti3AlC2 and Cr2AlC in air", Mater. Res. Lett. 1 (2013) 115–125. DOI:10.1080/21663831.2013.806364

[42] J. Gonzalez- Julian, I. Kraleva, M. Belmonte, F. Jung, T. Gries, R. Bermejo, "Multifunctional performance of Ti_2AlC MAX phase/2D braided alumina fiber laminates", J. Am. Ceram. Soc. 105 (2022) 120‑130. DOI: 10.1111/jace.18043

[43] T. C. Duong, A. Talapatra, W. Son, M. Radovic, R. Arróyave, "On the stochastic phase stability of Ti2AlC-Cr_2AlC", Sci. Rep. 7 (2017) 5138. DOI:10.1038/s41598-017-05463-1

[44] X. Li, S. Badie, J. Gonzalez-Julian, R. Schwaiger, J. Malzbender, "Abrasive behavior of M_2AlX MAX phase materials and its relation to the brittleness index", Ceram. Int. 48 (2022) 19501-19506. DOI: 10.1016/j.ceramint.2022.03.196

[45] T. Liao, J. Wang, Y. Zhou, "Chemical bonding and mechanical properties of M_2AC (M = Ti, V, Cr,A = Al, Si, P, S) ceramics from first-principles investigations", J. Mater. Res. 24 (2009) 556-564. DOI: 10.1557/JMR.2009.0066

[46] M.W. Barsoum, D. Brodkin, T. El-Raghy, "Layered machinable ceramics for high temperature applications", Scr. Mater. 36 (1997) 535-541. DOI:10.1016/S1359-6462(96)00418-6

[47] W.B. Zhou, B.C. Mei, J.Q. Zhu, X.L. Hong, "Rapid synthesis of Ti_2AlC by spark plasma sintering technique", Mater. Lett. 59 (2005) 131–134. DOI:10.1016/j.matlet.2004.07.052

[48] W. Ping, B.-C. Mei, X.-L. Hong, W.-B. Zhou, "Synthesis of Ti2AlC by hot pressing and its mechanical and electrical properties", Trans. Nonferrous Met. Soc. China. 17 (2007) 1001–1004.

DOI:10.1016/S1003-6326(07)60215-5

[49] L. Cai, Z. Huang, W. Hu, S. Hao, H. Zhai, Y. Zhou, "Fabrication, mechanical properties, and tribological behaviors of Ti_2AlC and $Ti_2AlSn_{0.2}C$ solid solutions", J. Adv. Ceram. 6 (2017) 90–99. DOI:10.1007/s40145-017-0221-9

[50] Z.J. Lin, M.S. Li, J.Y. Wang, Y.C. Zhou, "High-temperature oxidation and hot corrosion of Cr_2AlC", Acta Mater. 55 (2007) 6182–6191. DOI:10.1016/j.actamat.2007.07.024

[51] W. Tian, P. Wang, G. Zhang, Y. Kan, Y. Li, D. Yan, "Effect of composition and processing on phase assembly and mechanical property of Cr2AlC ceramics", Mater. Sci. Eng. A 454–455 (2007) 132–138. DOI:10.1016/j.msea.2006.11.032

[52] W. Tian, P. Wang, G. Zhang, Y. Kan, Y. Li, "Mechanical Properties of Cr_2AlC Ceramics", J. Am. Ceram. Soc. 90 (2007) 1663‑1666. DOI: 10.1111/j.1551-2916.2007.01634.x

[53] G. Ying, X. He, M. Li, W. Han, F. He, S. Du, "Synthesis and mechanical properties of high-purity Cr_2AlC ceramic", Mater. Sci. Eng. A 528 (2011) 2635–2640. DOI:10.1016/j.msea.2010.12.039

[54] S.B. Li, W.B. Yu, H.X. Zhai, G.M. Song, W.G. Sloof , S. van der Zwaag, "Mechanical properties of low temperature synthesized dense and fine-grained Cr2AlC ceramics", J. Euro. Ceram. Soc. 31 (2011) 217–224. DOI:10.1016/j.jeurceramsoc.2010.08.014

[55] E. Tabares, M. Kitzmantel, E. Neubauer, A. Jimenez-Morales, S. A. Tsipas, "Sinterability, Mechanical Properties and Wear Behavior of Ti_3SiC_2 and Cr_2AlC MAX Phases", Ceramics 2022, 5, 55–74. DOI:10.3390/ceramics5010006

[56] L. Qu, G. Bei, M. Nijemeisland, D. Cao, S. van der Zwaag, W. G. Sloof, "Point contact abrasive wear behavior of MAX phase materials", Ceram. Int. 46 (2020) 1722-1729. DOI:10.1016/j.ceramint.2019.09.145

[57] C.-F. Du, Y. Xue, Q. Zeng, J. Wang, X. Zhao, Z. Wang, C. Wang, H. Yu, W. Liu, "Mo-doped Cr-Ti-Mo ternary o-MAX with ultra-low wear at elevated temperatures", J. Euro. Ceram. Soc. 42 (2022) 7403–7413. DOI:10.1016/j.jeurceramsoc.2022.09.020

[58] C. Magnus, D. Cooper, J. Sharp, W. M. Rainforth, "Microstructural evolution and wear mechanism of Ti_3AlC_2 – Ti_2AlC dual MAX phase composite consolidated by spark plasma sintering (SPS)", Wear 438-439 (2019) 203013. DOI:10.1016/j.wear.2019.203013

[59] S. Gupta, M.W. Barsoum, "On the tribology of the MAX phases and their composites during dry sliding:A review", Wear 271 (2011) 1878–1894. DOI:10.1016/j.wear.2011.01.043

[60] S. Gupta, D. Filimonov, T. Palanisamy, M.W. Barsoum, "Tribological behavior of select MAX phases against Al2O3 at elevated temperatures", Wear 265 (2008) 560–565. DOI:10.1016/j.wear.2007.11.018

[61] I. Yu. Buravlev, A.A. Vornovskikh, O.O. Shichalin, A.O. Lembikov, T.L. Simonenko, A.I. Seroshtan, A.A. Buravleva, A.A. Belov, D. Yu Kosyanov, E.K. Papynov, “Reactive spark plasma synthesis of Mo2C/Mo3Co3C ceramic for heterostructured electrodes used for hydrogen energy technology”, Ceram. Int. 50 (2024) 14445–14457. DOI:10.1016/j.ceramint.2024.01.357

[62] M. Chmielewski, S. Nosewicz, E. Wyszkowska, Ł. Kurpaska, A. Strojny-Nędza , A. Piątkowska, P. Bazarnik, K. Pietrzak, "Analysis of the micromechanical properties of copper-silicon carbide composites using nanoindentation measurements", Ceram. Int. 45 (2019) 9164–9173. DOI:10.1016/j.ceramint.2019.01.257

[63] M. Chmielewski, S. Nosewicz, Ł. Kurpaska, B. Romelczyk, " Evolution of material properties during the sintering process of Cr-Re-Al2O3 composites", Composites Part B 98 (2016) 88-96. DOI:10.1016/j.compositesb.2016.04.065

[64] B. Tunca, T. Lapauw, R. Delville, D. R. Neuville, L. Hennet, D. Thiaudiere, T. Ouisse, J. Hadermann, J. Vleugels, K. Lambrinou, “synthesis and Characterization of Double Solid Solution $(Zr,Ti)_2(Al,Sn)C$ MAX Phase Ceramics”, Inorg. Chem. 58 (2019) 6669-668. DOI:10.1021/acs.inorgchem.9b00065

[65] M.A. Hadi, U. Monira, A. Chroneos, S.H. Naqib, A.K.M.A. Islam, N. Kelaidis, R.V. Vovk, “Phase stability and physical properties of $(Zr_{1-x}Nb_x)_2AlC$ MAX phases”, J. Phys. Chem. Solids 132 (2019) 38–47. DOI:10.1016/j.jpcs.2019.04.010

[66] Z. Liu, E. Wu, J. Wang, Y. Qian, H. Xiang, X. Li, Q. Jin, G.Sun, X. Chen, J. Wang, M. Li, “Crystal structure and formation mechanism of (Cr2/3Ti1/3)3AlC2MAX phase”, Acta Materialia 73 (2014) 186–193. DOI:10.1016/j.actamat.2014.04.006

[67] Z. Liu, L. Zheng, L. Sun, Y. Qian, J. Wang, M. Li, “(Cr2/3Ti1/3)3AlC2 and (Cr5/8Ti3/8)4AlC3: New MAX-phase Compounds in Ti–Cr–Al–C System”, J. Am. Ceram. Soc. 97 (2014) 67–69. DOI: 10.1111/jace.12731

[68] E.N. Hoffman, D.W. Vinson, R.L. Sindelar, D.J. Tallman, G. Kohse, M.W. Barsoum, "Max phase carbides and nitrides: Properties for future nuclear power plant in-core applications and neutron

transmutation analysis", Nuc. Eng. Design 244 (2012) 17–24. DOI:10.1016/j.nucengdes.2011.12.009

[69] Z. Sun, R. Ahuja, J. M. Schneider, "Theoretical investigation of the solubility in .$M_xM'_{2-x}$.AlC (M and M'=Ti,V,Cr)", PHYS. REV. B 68 (2003) 224112. DOI:10.1103/PhysRevB.68.224112

[70] G. Ying, X. He, S. Du, Y. Zheng, C. Zhu, Y. Wu, C. Wang, "Kinetics and numerical simulation of self-propagating high-temperature synthesis in Ti–Cr–Al–C systems", Rare Met. (2014). DOI:10.1007/s12598-013-0205-z

[71] L. Shang, D. Music, M. to Baben, J. M. Schneider, "Phase stability predictions of $(Cr_{1-x},M_x)_2(Al_{1-y},A_y)(C_{1-z},X_z)$ (M = Ti, Hf,Zr; A = Si, X = B)", J. Phys. D: Appl. Phys. 47 (2014) 065308. DOI:10.1088/0022-3727/47/6/065308

[72] D. Horlait, S. Grasso, N. Al Nasiri, P. A. Burr, W. E. Lee, "Synthesis and Oxidation Testing of MAX Phase Composites in the Cr–Ti–Al–C Quaternary System", J. Am. Ceram. Soc. 99 (2016) 682‑690. DOI: 10.1111/jace.13962

[73] G. Ying, X. He, M. Li, Y. Li, S. Du, "Synthesis and mechanical properties of nano-layered composite", J. Alloys Compd. 506 (2010) 734–738. DOI:10.1016/j.jallcom.2010.07.057

[74] H. Wang, Z. Huang, X. Li, Q. Yu, W. Hu, W. Zhuang, Y. Wu, Y. Zhou, “Reaction mechanism and microstructure evolution of superhigh strength in-situ TiC/Ti composite based on Cr2AlC-Ti system”, J. Alloys Compd. 965 (2023) 171524. DOI:10.1016/j.jallcom.2023.171524

[75] C.-S. Kim, S. Ik Hwang, J.-S. Ha, S.-M. Kang, D.-S. Cheong, “Synthesis of a Cr_2AlC-Ti_2AlC ternary carbide”, J. Ceram. Proc. Res. 11 (2010) 82-85. https://kiss.kstudy.com/DetailOa/Ar?key=51126040

[76] A. Olejarz, W.Y. Huo, M. Zieliński, R. Diduszko, E. Wyszkowska, A. Kosińska, D. Kalita, I. Jóźwik, M. Chmielewski, F. Fang, Ł. Kurpaska, "Microstructure and mechanical properties of mechanically-alloyed CoCrFeNi high-entropy alloys using low ball-to-powder ratio", J. Alloys Compd. 938 (2023) 168196. DOI:10.1016/j.jallcom.2022.168196

[77] A. Olejarz, W. Huo, D. Kalita, M. Zieliński, E. Wyszkowska, W. Chromiński, R. Diduszko, M. Chmielewski, I. Jóźwik, Ł. Kurpaska, " Cr-rich structure evolution and enhanced mechanical properties of CoCrFeNi high entropy alloys by mechanical alloying", J. Mater. Res. Tech. 30, May–June 2024, Pages 1490-1504. DOI: 10.1016/j.jmrt.2024.03.116

[78] Standard Test Methods for Density of Compacted or Sintered Powder Metallurgy (PM) Products Using Archimedes’ Principle, (2023). DOI:10.1520/B0962-23

[79] G.M. Pharr, W.C. Oliver, "Measurement of Thin Film Mechanical Properties Using Nanoindentation", MRS Bulletin. 17 (1992) 28-33. DOI:10.1557/S0883769400041634

[80] Standard Test Method for Wear Testing with a Pin-On-Disc Apparatus, (2010). DOI:10.1520/G0099-05

[81] M. Ghanbariha, M. Farvizi, T. Ebadzadeh, A. Alizadeh Samiyan, "Effect of ZrO2 particles on the nanomechanical properties and wear behavior of AlCoCrFeNi–ZrO2 high entropy alloy composites". Wear 484-485 (2021) 204032. DOI:10.1016/j.wear.2021.204032

[82] Y. Yang, H. Lu, C. Yu, J.M. Chen, “First-principles calculations of mechanical properties of TiC and TiN”, J. Alloys Compd. 485 (2009) 542‑547. DOI:10.1016/j.jallcom.2009.06.023

[83] L. Sun, X. Ji, L. Zhao, W. Zhai, L. Xu, H. Dong, Y. Liu, J. Peng, “First Principles Investigation of Binary Chromium Carbides Cr7C3, Cr3C2 and Cr23C6: Electronic Structures, Mechanical Properties and Thermodynamic Properties under Pressure”, Materials 15 (2022) 558. DOI:10.3390/ma15020558

[84] S.A. Ataie, M. Soltanieh, R. Naghizadeh, A. Cavaleiro, M. Evaristo, F. Fernandes, F. Ferreira, "Effect of substrate bias voltage on structural and tribological properties of W-Ti-C-N thin films produced by combinational HiPIMS and DCMS co-sputtering", Wear 520–521 (2023) 204654. DOI:10.1016/j.wear.2023.204654

[85] S.A. Ataie, M. Soltanieh, R. Naghizadeh, A. Cavaleiro, F. Fernandes, F. Ferreira, “Effect of peak power on microstructure, mechanical and tribological properties of W-Ti-C-N(O) ceramic films produced by hybrid sputtering”, Trib. Int. 189 (2023) 108983. DOI:10.1016/j.triboint.2023.108983

[86] K. Vijaya Bhaskar, S. Sundarrajan, B. Subba Rao, K. Ravindra, “Effect of reinforcement and wear parameters on dry sliding wear of aluminum composites - A review”, Mater. Today 5 (2018) 5891-5900. DOI:10.1016/j.matpr.2017.12.188

[87] Z. T. Y. Liu, D. Gall, S. V. Khare, " Electronic and bonding analysis of hardness in pyrite-type transition-metal pernitrides", PHYS. REV. B 90 (2014) 134102. DOI:10.1103/PhysRevB.90.134102